Article

A Multi-Level World Comprehensive Neural Network Model for Maximum Annual Solar Irradiation on a Flat Surface

Ramez Abdallah [1] , **Emad Natsheh** [2] , **Adel Juaidi** [1,*] , **Sufyan Samara** [2] **and Francisco Manzano-Agugliaro** [3,*]

[1] Department of Mechanical Engineering, Faculty of Engineering & Information Technology, An-Najah National University, P.O. Box 7 Nablus, Palestine; ramezkhaldi@najah.edu

[2] Department of Computer Engineering, Faculty of Engineering & Information Technology, An-Najah National University, P.O. Box 7 Nablus, Palestine; e.natsheh@najah.edu (E.N.); sufyan_sa@najah.edu (S.S.)

[3] Department of Engineering, University of Almeria, ceiA3, 04120 Almeria, Spain

[*] Correspondence: adel@najah.edu (A.J.); fmanzano@ual.es (F.M.-A.)

check for updates

Abstract: With the growing demand for clean and economically feasible renewable energy, solar photovoltaic (PV) system usage has increased. Among many factors, the tilt and azimuth angles are of great importance and influence in determining the photovoltaic panel's efficiency to generate electricity. Although much research was conducted related to solar PV panels' performance, this work critically determined the tilt and azimuth angles for PV panels in all countries worldwide. The optimum tilt and azimuth angles are estimated worldwide by the photovoltaic geographic information system (PVGIS). Also, annual and average daily solar irradiation incident on the tilted and oriented plate optimally (AR1 and DR1) are calculated. Besides, annual and average daily solar irradiation incident on plate tilt optimally and oriented because of the south in the northern hemisphere and because of the north in the southern hemisphere (AR2 and DR2) are estimated. PVGIS is also used to calculate the annual and average daily solar irradiation incident on the horizontal plate (AR3 and DR3). The data collected from PVGIS are used to develop an efficient and accurate artificial neural network model based on feed-forward neural network approach. This model is an essential subpart that can be used in an embedded system or an online system for further PV system analysis and optimization. The developed neural model reflected very high accuracy in predicting the PV panels' optimal tilt and azimuth angles worldwide. The benefit of tilting is generally increased by increasing the latitude. As the latitude increases, the tilt factor (F) increases because of the increase in the optimum tilt angle by increasing the latitude. The optimal orientation is due to the north in the southern hemisphere and due to the south in the northern hemisphere for most cities worldwide. In sum, it can be concluded that the optimum tilt angle is equal to or greater than the latitude until the latitude 30°. The optimum tilt angle becomes less than the latitude, and the difference is increased until it reaches more than 20°. Hence in this study the aim is to develop a simple neural network model which can accurately predict the annual radiation and optimum tilt and azimuth angle in any region of the world and can be easily implemented in a low-cost microcontroller.

Keywords: optimal tilt angle; PV system; solar photovoltaic; solar irradiation; Levenberg Marquardt algorithm; feed-forward neural network

1. Introduction

Solar energy is considered as an original and unlimited source of energy and it also works to enhance energy security and sustainability, and this in turn leads to reducing pollution; also, to keep the prices of fossil fuels lower than others. It also reduces the cost of mitigating climate change [1,2]. Thus, according to IRENE [3], the production of solar photovoltaic (PV) energy is increasing annually. For example, the existing solar PV energy production increased more than 27 times from the production ten years ago; in 2009, it was less than 23 gigawatts. The solar PV installation capacity reached 627 gigawatts in 2019 compared to 512 in 2018 [3].

Because of rapid technological progress and reduce costs, solar PV will have an essential role in reaching the sustainable development goals (SDGs) by 2030 [4], increase the share of renewable energy in the universal electricity sector, in addition to the provision of electricity for remote areas [5–9].

The amount of solar energy produced by a solar PV panel can be determined based on the local insolation. However, it is affected by the solar PV panels' tilt and orientation angles [10–13]. Thus, an appropriate tilt and orientation angle must be applied to achieve the maximum produced energy for a specific location [14–17]. Although one can use a solar tracking system that follows the sun to receive the maximum amount of daily energy, on the other hand, solar tracking systems are expensive and additional energy is needed for its operation [2].

Thus, it is commonly convenient to fix the solar PV on an optimum orientation and tilt angle [18–20]. Therefore, solar PV panels are recommended to be placed at the optimum tilt and orientation angle to obtain the yearly maximum energy production [10,11].

Many authors have attempted various analytical, simulations, and experimental work to obtain the optimum angles [21,22]. A general approximate rule for optimizing angles is that a given location's tilt angle is approximately equal to its latitude. The orientation angle should be south for Northern Hemisphere and north for Southern Hemisphere [23].

The present study used data from the Photovoltaic Geographical Information System (PVGIS), 2019 [24] for estimating optimum angles. The PVGIS gives solar irradiation on a horizontal surface and a surface tilted from horizontal or oriented because of the south. Moreover, the PVGIS provides an optimum tilt and azimuth angle that give the maximum yearly solar irradiation. The PVGIS is employing irradiation data based on satellite images. Based on satellite images, all databases provide hourly solar irradiation estimates. This means that PVGIS can be employed for any place, no matter how far from particular meteorological stations.

This study aims to find an artificial neural network model that can calculate an optimum tilt and azimuth angle in any world region. This model can be used inside an embedded system or as an online service. For an artificial neural network to be constructed and trained, it is required to obtain data from many locations worldwide.

The used data are obtained by PVGIS. First, the optimum tilt angles that give the maximum yearly solar irradiation for surfaces directed because of the south in the northern hemisphere and north in the southern hemisphere are calculated. Second, the optimum azimuth angles accompanying the optimum tilt angle are also calculated. Third, the annual and average daily irradiation in different regions all over the world is calculated for surfaces tilted with optimum tilt angles and directed because of the south in the northern hemisphere and because of north in the southern hemisphere (AR2 and DR2) and surfaces tilted with optimum tilt angle and oriented with optimum azimuth angles (AR1 and DR1). Fourth, the annual and average daily irradiations for horizontal surfaces are calculated (AR3 and DR3). Lastly, the tilt fact (F), which can be defined as the ratio of the irradiation collected by a tilted surface to the irradiation collected by a horizontal surface, is calculated.

Although one can use mathematical or statistical modules to calculate that based on some rules or conditions, these approaches tend to be very difficult and inaccurate when such conditions are hard to predict, has a non-linear form, or with a pattern that is hard to find [25]. Adding to that, for their hardware implementation they require expensive microcontrollers.

The best output energy of a PV panel depends mainly on the maximum vertical amount of solar radiation that hits the PV panel surface. This maximum vertical solar irradiation changes according to the tilt and azimuth angles. Artificial intelligence can help increase this amount of solar irradiation by finding optimum tilt and azimuth angles, which is challenging to model accurately using mathematical or statistical modules, even for a single location [26].

Neural networks are characterized by being capable to learn by themselves and produce an output that is not limited to the input provided to them. Moreover, even if a neuron is not responding or a piece of information is missing, the network can detect the fault and still produce the output. Hence in this study, the aim is to develop a simple neural network model that can accurately predict the annual irradiation and optimum tilt and azimuth angle in any region of the world and can be easily implemented in a low-cost microcontroller.

2. Literature Review

Obtaining the photovoltaic system's optimum tilt angle is a significant issue because it helps to effectively transform the amount of sunlight received into energy [27]. Numerous studies have used various research approaches to find a tilt angle that maximizes the amount of irradiation received by the solar panel [27]. Such models include Hay's model, PVsyst simulation, PV-Simulation model, Nijegorodov equations, Harmony search meta-heuristic algorithm, PVWatts program, PVGIS program, particle swarm optimization (PSO) estimator, analytical method, MATLAB software, Oracle Crystal Ball software, and Gradient Boosting Algorithm. Table 1 summarizes these methods.

Kim Gi et al. [11] used a machine learning approach to find the optimum tilt angle of a PV panel to maximize the energy obtained from the PV panel. Although the analysis was conducted in a single area, and all PV panels shared similar geometric attributes, the optimal angles varied to certain degrees.

Artificial intelligence techniques can be employed in many problems. Their importance is realized in the ability to learning and adapt to new variations efficiently. This ability makes these techniques a promising solution in finding optimum tilt and azimuth angles for PV panels worldwide with high accuracy. While some attempts to explore the benefits these techniques offer [26,27], there is insufficient research in this field for such techniques.

This research provides an estimate of optimum tilt angles for (PV) panels for all countries worldwide.

Table 1. Shows the optimum tilt angles using different methods for several countries worldwide from 1988 to 2020.

Country or Region	City	Latitude (φ) (°)	Optimum Tilt Angle (β) (°) Annually	Reference
Jordan	Mu'tah	31.7	28.5	A mathematical model is developed [28].
Egypt	Assiut	27.2	27	Moncos (1994) developed a mathematical model [29].
Spain	Valencia	28.5	31	The Hay model was used to assess the hourly variance of the optimal tilt angle for a solar collector facing south and to measure the annual average of this angle [30].
Darussalam	Brunei	4.5	3.3	A mathematical model was used [31].
China	Beijing	39.9	39.2	A mathematical model is developed [32].
	Kunming	24.9	27.9	
	Shanghai	31.2	28	
	Guangzhou	23.1	22	
	Chengdu	30.6	23	
	Xi'an	34.3	30.1	
	Yinchuang	38.5	38.3	
	Shenyang	41.8	40.3	
Turkey	Izmir	38.4	June: 0 December: 61	A mathematical model is developed [33].
Syria	Damascus	33.5	30.56	A mathematical model is used [34].
Iran	Zahedan	29.5	26.70	A more precise equation than the Nijegorodov one is formed to measure the monthly optimum tilt angle using a new correlation for each month [35].
	Birjand	32.9	29.93	
	Shraz	52.9	25.88	
	Tabas	33.6	30.16	
	Yazd	31.9	29.05	
	Kerman	36.7	23.95	
Mediterranean Region	Gaza Strip (Palestine)	31.5	32.1	As a function of the tilt angle, a mathematical model is used to measure the solar radiation on a tilted surface [36].
	Damascus (Syria)	33.5	33.7	
	Beirut (Lebanon)	33.9	33.8	
	Tunis (Tunisia)	33.9	35.2	
	Seville (Spain)	37.4	36.6	
	Milan (Italy)	45.5	41.8 Summer: $\beta = \varphi - 15°$ Winter: $\beta = \varphi + 15°$	
Jordan	Northern Jordan	32.5°	30 Summer: 10 Winter: 50	Based on the results of the PVsyst simulation for Northern Jordan [37].

Table 1. *Cont.*

Austria and Germany	Germany	51.2	30–45	A PV-simulation model is provided for the measurement of angle-dependent PV performance. For Germany and Austria, a linear power and simplified dispatch model was calibrated and used [38].
	Austria	47.5	30–45	A PV-simulation model is provided for the measurement of angle-dependent PV performance. For Germany and Austria, a linear power and simplified dispatch model was calibrated and used [38].
Iran	Tehran	35.7	35.7	For measuring solar radiation on a tilted surface, a mathematical model is suggested. The maximum angle of incidence is detected using the Gravitational Search Algorithm (GSA) [39].
	Isfahan	36.5	32	
	Shiraz	29.6	29.4	
	Mashhad	36.3	36.2	
	Tabriz	38.1	38	
Kosovo	Pristina	42.7	34.7 Summer: 8.9 Spring: 25.7 Autumn: 50.9 Winter: 62.1	Based on isotropic sky analysis models, namely Liu and Jordan models, the incident plane's solar radiation is calculated [40].
China	Sanya	11.5	−18 (June) to 49.9 (Dec.)	The algorithm Harmony (meta-heuristic) determines the azimuth angle and optimum tilt [41]. The findings are built on the ergodic mechanism [41].
	Shanghai	31.2	−7.6 (June) to 61.4 (Dec.)	
	Zhengzhou	34.7	5.5 (June) to 64.3 (Dec.)	
	Harbin	45.8	12.6 (June) to 73.7 (Dec.)	
	Mohe	52.9	16.6 (June) to 80.0 (Dec.)	
	Lhasa	29.7	−8.9 (June) to 59.9 (Dec.)	
All Countries Worldwide	Canada (Montreal)	45.5	37	This study uses the PVWatts program to calculate the optimal tilt angles for all countries worldwide [42].
	Bordeaux (France)	44.8	33	
	Cologne (Germany)	50.9	32	
	Hong Kong	22.4	20	
	Rajko (India)	42.1	24	
	Beek (Netherlands)	50.9	34	
	Castellón (Spain)ón	39.1	36	
	Austin, TX (United States)	30.3	28	
	London (United Kingdom)	51.5	34	
	Jerusalem (Palestine)	31.8	28	
	Casablanca (Morocco)	33.6	28	
	Beirut (Lebanon)	33.9	28	
	Kuwait City (Kuwait)	29.3	26	
	Amman (Jordan)	31.9	28	
	Tehran (Iran)	35.68	31	
	Aswan (Egypt)	24.1	24	
	Abu Dhabi (United Arab Emirates)	24.5	25	

Table 1. *Cont.*

Country	City	φ	Optimal Tilt	Method
Cyprus	Famagusta	35.1	28 to 30 Summer: 20 Winter: 50	PV simulation software will be used to determine the average solar radiation on different tilt. From this, to assess an optimal tilt angle, the peak annual average solar radiation shall be obtained on various tilted surfaces [43].
Palestine	West Bank Gaza Strip	31.9	29	1. For determining the optimum tilt angle, a mathematical model is used [20].
				2. PVWatts 3. PVGIS
India	Minicoy Ahmadabad New Delhi	8.3 23.0 28.6	Analytical PSO Estimator 11.00 10.51 26.00 25.83 27.00 26.92	1. To find an optimal tilt angle, a model-driven optimization focus has been proposed, such as a particle swarm optimization (PSO) estimator [44] 2. Analytical method
Ghana	Kumasi	6.7	10	System simulation RETScreen 4. For all the three systems' orientation, the electrical energy output produced by the solar module was calculated [45].
Turkey	Antalya Kayseri Trabzon	36.9 38.7 41.0	Winter: $\beta = \varphi + 17°$ Spring: $\beta = \varphi - 18°$ Summer: $\beta = \varphi - 34°$ Autumn: $\beta = \varphi + 7°$ Annual: $\beta = \varphi - 7°$	For the Northern Hemisphere and sample provinces, various mathematical models have been developed. PVGIS, NASA, and other approaches [46].
Iran	Bandar Abbas Yazd Isfahan Tehran Urmia	27.13 31.54 32.57 35.41 37.32	18.84 21.47 22.04 23.59 23.27 $\beta = 0.4663\varphi + 6.5489°$	The optimal tilt angle is calculated using a distributed software developed on MATLAB. Based on particle swarm optimization (PSO) approach [47].
Indonesia	Bukit Jimbaran Bali	5.4	φ from 12–18 in the azimuth of 0. (Apr. to Sep.): 32 (Oct. to Mar.): 24	Simulations found that for fixed solar panels in a year. Data of solar radiation and the simulation of PV system are from Metronome 7.2 [48].
USA	Eaton County, Michigan	39.7	42.7	Oracle Crystal Ball program using Microsoft Excel (OptQuest Solver Engine) was used to calculate optimal tilt angles [49].
South Korea	Daegu City	35.9	1 to 29	Optimization model using machine learning algorithms: Gradient Boosting Algorithm [27].
Norway France Egypt Kenya	Trondheim Paris Cairo Nairobi	63.4 48.9 30.0 −1.3	52 43 29 3	A proposed approach to use real historical solar spectra to test a panel's tilt at a given location rigorously [50].

3. Methodology

In this work, an artificial neural network is used to find the optimum tilt and azimuth angles that yield maximum energy from PV panels in any worldwide location. To effectively build such neural networks, training data is sampled from many locations worldwide using PVGIS (Photovoltaic Geographical Information System, 2019) [24]. PVGIS provides solar irradiation on a horizontal surface and a surface tilted from horizontal or oriented because of the south. Moreover, the PVGIS provides an optimum tilt and azimuth angle that gives the maximum yearly solar irradiation. The PVGIS employs irradiation data based on satellite images. Satellite images are used to collect solar irradiation data. The different satellites available in PVGIS are:

- PVGIS-SARAH: CM SAF [51] and the PVGIS [24] team have calculated these data covering Europe, Africa, most of Asia, and parts of South America.
- PVGIS-NSRDB: These data have been supplied by the National Renewable Energy Laboratory (NREL) [52] and is part of the National Solar Irradiation Database.
- PVGIS-CMSAF: CM SAF collaboration [51] have calculated these data covering Europe, Africa, and parts of South America.
- PVGIS uses two more satellites to cover high-latitude areas not covered by previous satellites.
- PVGIS-ERA5: This new re-analysis product is obtained from ECMWF [53]. It covers all over the world on an hourly basis and is used by PVGIS for Europe.
- PVGIS-COSMO: COSMO-REA6 is a regional re-analysis product, covering Europe at hourly time resolution.

Based on the satellite images, all databases provide hourly solar irradiation estimates. This means that PVGIS can be employed for any place, no matter how far from particular meteorological stations.

The PVGIS is used to obtain data for training and validating the developed artificial neural network model. Figure 1 shows the locations around the world used to gather training data.

Figure 1. The places where the training data are collected.

In Figure 1, the locations are highlighted by colored circles. The circles' color is separated to give the figure more detail, and they do not mean anything else.

The development of the artificial neural network model is carried out using feed-forward neural networks (FFNN). The development process is divided into the training phase and the testing phase. Figure 2 shows the methodology used to develop the FFNN model.
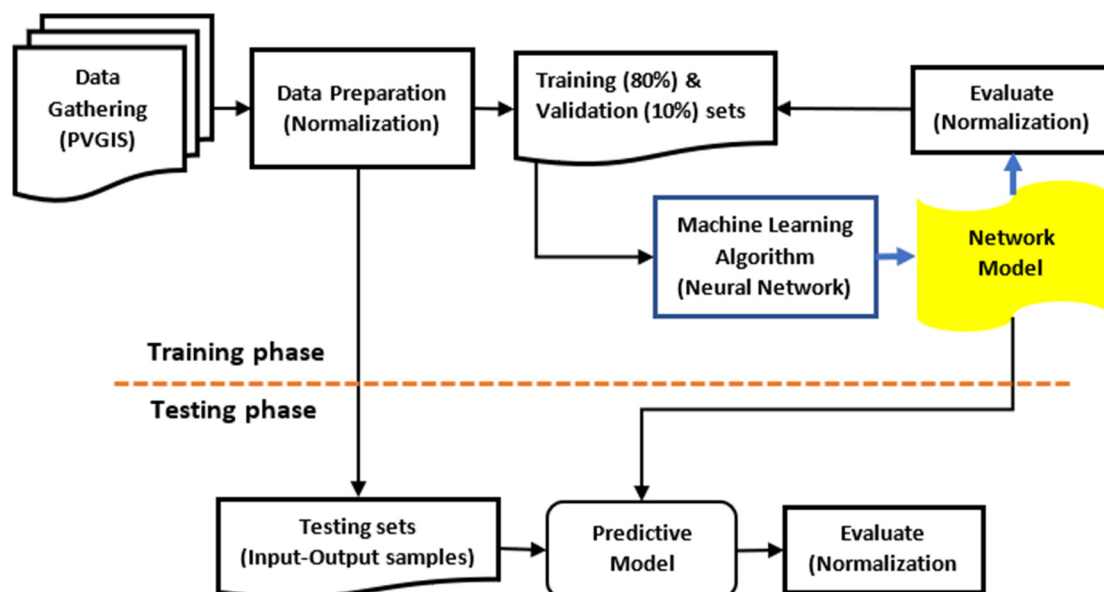
Figure 2. Methodology used to develop the feed-forward neural networks (FFNN) model.

The data collected were normalized and divided into two sets after the correct validation using the PVGIS method. One was used at the development stage of the neural model, representing 90% of the data collected, and one was used at the neural model test stage, representing around 10%. The testing phase aims to evaluate the neural network model developed in the training phase. The 90% of the gathered data used in the training phase was further divided into a neural network model training set, about 80% of the gathered data, and a neural network model validating set, which is about 10% of the gathered data. After the training phase, a multi-level FFNN model was developed. The developed multi-level FFNN model is discussed in the subsequent section.

Multi-Level Neural Network Model

Feed-forward neural network (FFNN) is a supervised learning algorithm that learns, by training on a dataset, a function $f(.) : R^n \rightarrow R^o$. Where o is the number of dimensions for output, and n is the number of dimensions for inputs. Given a set of features $X = \{x_1, x_2, \ldots, x_n\}$ and targets $Y = \{y_1, y_2, \ldots, y_o\}$, it can learn a non-linear function approximator for either regression or classification problems. In this work, FFNN is used as a regression model, and this differs from logistic regression, as there are one or more non-linear layers, called the hidden layer, which lies between the input and output layers. Figure 3 shows one hidden layer FFNN.

The leftmost layer, known as the input layer, consists of neurons expressing the input patterns, as shown in Figure 3. With a weighted linear summation $\sum_{i=1}^{n} x_i w_{ij}$, each neuron in the hidden layer transforms the previous layer's values, which are then evaluated using activation function [54]. Where w_{ij} is the weight relation between the *i*th neuron in the input layer and the *j*th neuron in the hidden layer, xi is the value of *i*th neuron in the input layer. The values are propagated to the neurons of the output layer to generate the output patterns.

Figure 4 shows the topology of the proposed model. The proposed network model predicts the PV's optimum tilt and azimuth angle of annual irradiation in various regions worldwide.
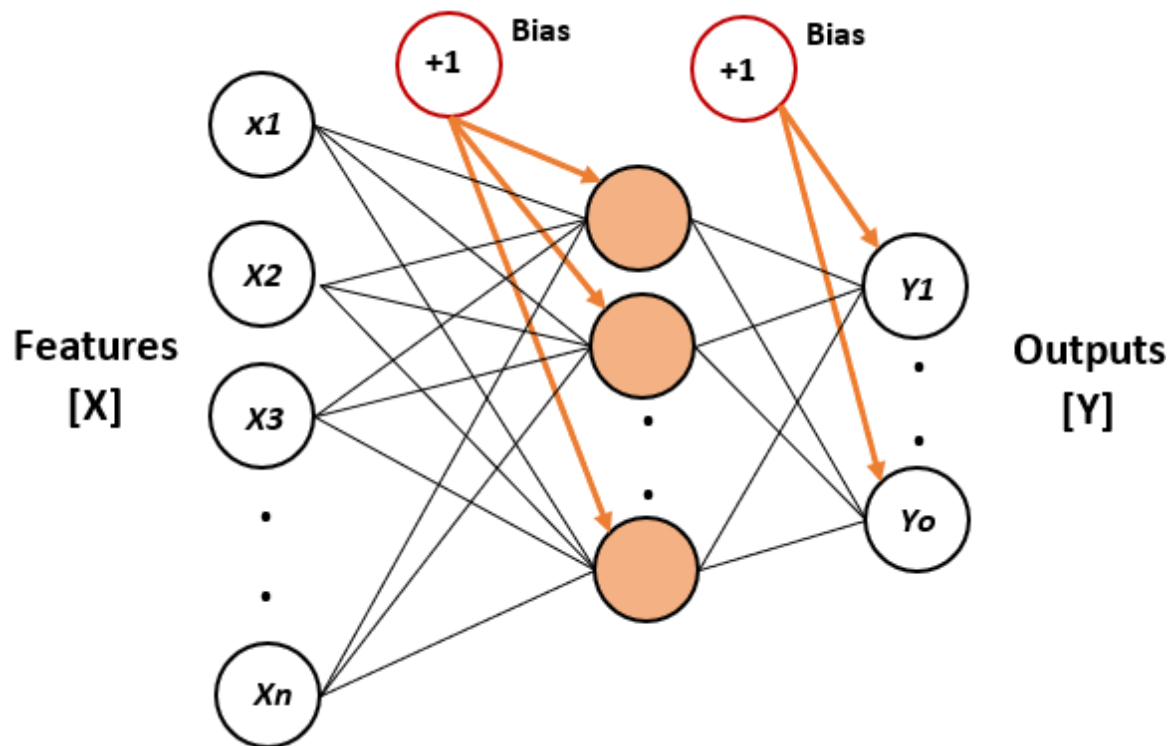
Figure 3. One hidden layer neural network structure.
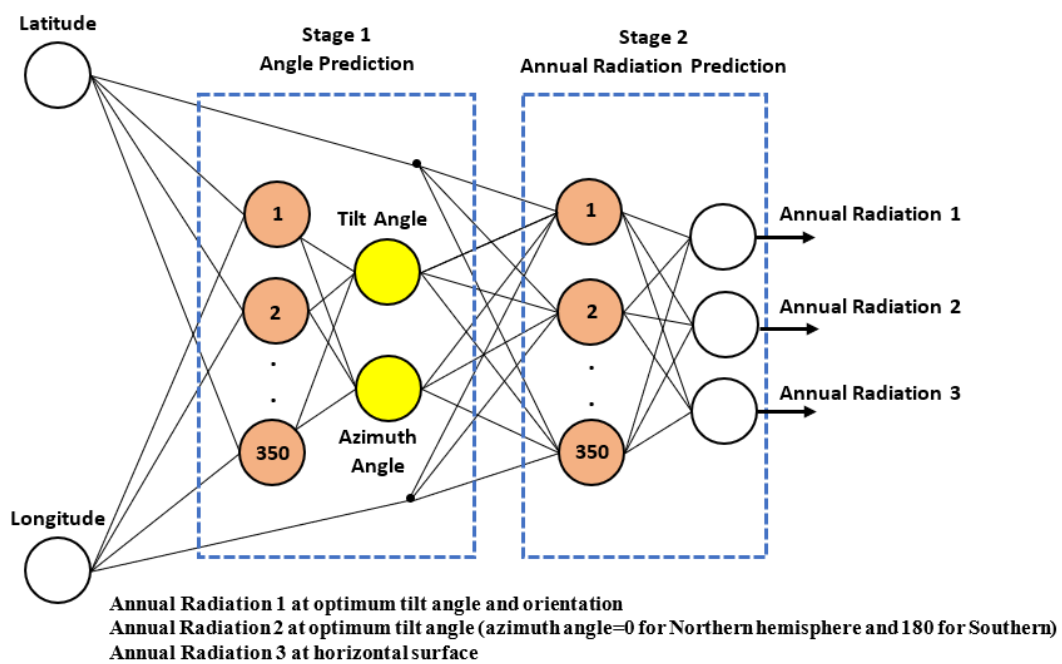
Figure 4. The developed neural network topology.

The proposed model is composed of two phases, as shown in Figure 4. The model consists of three layers in the first stage: Input, Hidden, and Output. Two nodes form the input layer: longitude (deg.) and latitude (deg.). Three hundred fifty nodes compose the hidden layer, each of which uses the activation function of the hyperbolic tangent sigmoid. The output layer consists of two nodes that evaluate the optimal PV's tilt and azimuth angles.

The second stage's input layer is composed of four nodes, two of them are the outputs of the first stage (tilt and azimuth angles), and the others are the Latitude and the Longitude. The hidden layer is like the first stage; it has 350 nodes with tanh activation function. At the same time, the output layer has three nodes, which are the annual irradiation under (1) optimum tilt angle and orientation (2) optimum tilt angle (azimuth angle = 0 for the Northern hemisphere and 180 for Southern) (3) horizontal surface. The output nodes in the two stages use an activation function of linear type [49].

Min-Max normalization method is used on all data to improve the qualified network's efficiency [55]. The data are then used to trained the network to understand the relationships between the input patterns.

$$I_N = (I - I_{min}) \left[\frac{N_{max} - N_{min}}{I_{max} - I_{min}} \right] + N_{min} \tag{1}$$

$$O = (O_N - N_{min}) \left[\frac{O_{max} - O_{min}}{N_{max} - N_{min}} \right] + O_{min} \tag{2}$$

where N_{min} and N_{max} are the Min-Max normalize range, O_{max} and O_{min} are the maximum and minima values for the O output vector, O_N and I_N are the normalized training output and input values, I_{max} and I_{min} are the maximum and minima values for the input vector I, and I and O are the non-normalized training input and output values. For this work, $N_{min} = -1$ and $N_{max} = 1$ [56].

Different types of FFNN's trained algorithms were developed [55,57,58]. These include the Gradient descent with momentum approach, the Levenberg-Marquardt (LM) backpropagation, the Gradient descent backpropagation, and the adaptive learning rate resilient scaled conjugate gradient backpropagation. The LM training algorithm has been chosen for this work for the training of the proposed network model. Since the less responsive approach to local converges, the LM teaching method offers a more robust learning training approach. It also offers a healthy trade-off between the pace of preparation and stability [55].

Figure 5 displays the pseudocode for the training algorithm. The goal is to minimize as much as possible, the mean square error (MSE) by tuning the parameter (μ) as follows:

- $\mu \times 0.1$ when the MSE is equal or less to the previous one.
- $\mu \times 10$ when the current epoch MSE exceeds the previous value.

Input: A training input vector (**I**_N), desired output vector (**O**_N)

Output: A vector of modified weights and Biases (**W**)

Algorithm:

Set all the weights and Bias levels of the network to random numbers uniformly distributed inside a small range $\left[-2.4/_{fi}, +2.4/_{fi} \right]$

Compute: $MSE = \dfrac{1}{n} \sum_{i=1}^{n} \left(Y_{vi} - \overline{Y_{vi}} \right)^2$,

while (not stop-criterion) **do**

Compute: $\Delta W = \left(J J^t + \mu I_m \right)^{-1} J^t e$,

Update the network weights (**W**) using ΔW

Recalculate **MSE** using the updated weights

if MSE decrease **then**
$$\mu = 0.1\mu$$

else

Discard the new weights
$$\mu = 10\mu$$

end if

end while

Figure 5. Levenberg Marquardt algorithm.

4. Results and Discussion

4.1. Results Obtained by PVGIS

In the first part of the paper, PVGIS was used to obtain the results and tabulated in Table A1 (Appendix A). The optimum tilt angles, optimum azimuth angle, AR1, DR1, AR2, DR2, AR3, DR3, and F, are calculated for the different regions worldwide.

It can be concluded that the tilt angle is equal to or greater than the latitude until the latitude of 30°, then the tilt angle becomes less than the latitude until the difference between them reaches more than 20°. The relation between them is not linear for all the latitudes because the linear relationship does not take into account the air pollution and cloud cover. As the cloud cover increases, the optimum tilt angle decreases because the cloud cover scatters the solar irradiation. The solar PV is closer to the horizontal as it receives more of the diffuse solar irradiation that is scattered by the cloud cover. Besides, the direct solar irradiation, which mainly depends on the tilt angle, is mostly blocked by clouds, so the diffuse irradiation becomes more critical in the overcast latitudes. The azimuth or orientation of the solar PV is measured from the south, meaning that if it is directed to the south, then the azimuth angle is 0°, while if it is directed to the north, then the azimuth angle is 180°. For the east, the azimuth is −90 degrees, and for the west, it is 90 degrees. It can be concluded that the optimum azimuth angle for most cities in the northern hemisphere and southern hemisphere is close to 0° and 180°, respectively. Even cities with an optimum azimuth angle further from 0° and 180° gain a little extra annual solar irradiation (AR1-AR2). This means that the solar PV can be directed toward the south in the northern hemisphere and toward the north in the southern hemisphere.

Table 1 shows that the annual solar irradiation increases as it moves away from the equator until it reaches the maximum point (25–30°) for latitude and then begins to decrease. It can also be noticed that the tilt factor (F) increases with increasing latitude because of the increase in the optimum tilt angle with latitude.

The results obtained from PVGIS are compared with many previous studies and the results are very close [59,60].

4.2. Evaluation of the Proposed Nural Network Model

Several experiments have been performed to determine the best composition of the neural network. The decisions were made based on two main features: the activation function for each layer and the neurons' number in the hidden layer. Table 2 shows the attributes of the selected configurations.

Table 2. The parameters of the proposed network models' structures.

Stage 1 Structure (Angle Prediction)		Stage 2 Structure (Annual Irradiation Prediction)	
Attribute	**Choice**	**Attribute**	**Choice**
Number of inputs	2	Number of inputs	4
Number of outputs	2	Number of outputs	3
The hidden layer activation function	Hyperbolic Tangent	The hidden layer activation function	Hyperbolic Tangent
Output layer activation function	Linear (Regression)	Output layer activation function	Linear (Regression)
Normalization interval of the dataset	$[-1, 1]$	Normalization interval of the dataset	$[-1, 1]$
Training approach	Levenberg-Marquardt	Training approach	Levenberg-Marquardt
Error	Mean Squared Error	Error	Mean Squared Error

Another important feature that has been studied to complete the neural network structures is the number of nodes in each hidden layer. Table 3 compares the mean square error (MSE) results in various hidden layer numbers for both network stages.

Table 3. The hidden layers number of neurons vs. best-obtained results.

	Stage 1 Structure (Angle Prediction)				Stage 2 Structure (Annual Irradiation Prediction)		
Nodes	**MSE Train**	**MSE Validation**	**MSE Test**	**Number of Nodes**	**MSE Train**	**MSE Validation**	**MSE Test**
100	12.5169	8.3296	17.861	100	50.6192	150.9851	212.771
150	7.8641	2.0191	11.218	150	13.8712	33.8164	41.831
200	4.0127	1.1729	6.071	200	2.1176	3.8155	7.981
250	3.810×10^{-1}	4.7263	5.291	250	6.1839×10^{-1}	1.0069	4.441
300	6.211×10^{-2}	2.1058×10^{-1}	8.16×10^{-1}	300	2.0174×10^{-2}	5.9816×10^{-2}	7.97×10^{-1}
350	2.527×10^{-2}	1.1688×10^{-3}	4.0×10^{-2}	350	7.3972×10^{-3}	1.5783×10^{-4}	6.26×10^{-3}
400	8.875×10^{-2}	4.6688×10^{-2}	1.94×10^{-1}	400	2.9261×10^{-3}	7.2705×10^{-3}	7.91×10^{-2}
300×300	2.1197×10^{-2}	8.9912×10^{-1}	1.368	300×300	4.2281×10^{-1}	2.8861×10^{-1}	1.891
350×350	7.9712×10^{-1}	9.1862×10^{-1}	2.261	350×350	8.6691×10^{-2}	7.6331×10^{-1}	3.225

The best-obtained configuration for models' stages 1 and 2 is 350 neurons the hidden layer, seen in Table 3. MSE for both first stage preparation, checking, and validation is 0.0253, 0.041, and 0.00117, respectively, and for the second stage is 0.0074, 0.0063, and 0.00016, respectively. However, the results did not get any higher, while the sophistication grew as we went to the deep neural network.

Once the network configuration was chosen and before the simulation started, the dataset of 573 cities was split into three sections: training (459 cases), validation (57 cases), and testing (57 cases) (57 cases). The dataset has been chosen in a way that covers the maximum possible area, according to

the map shown in Figure 1. Using the early stop technique and the validation **set** [61], the overfitting was reduced. Figure 6 demonstrates the consequences of both systems during training and validation.
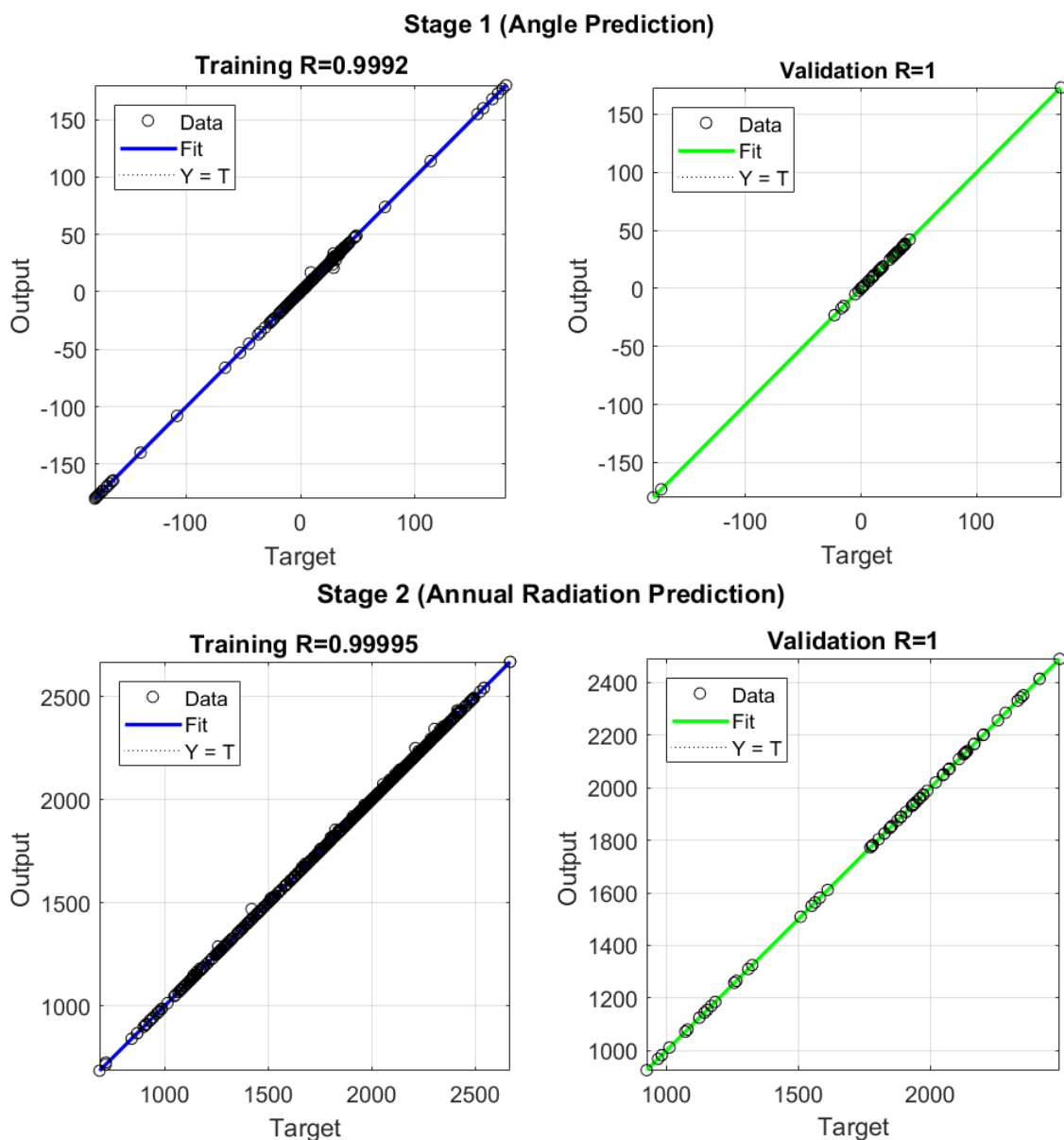
Figure 6. Regression of error for both stage 1 and 2 networks model.

As shown Figure 6, the linear regression for the training and validation of both models exactly matches the data sets, which means that the decision coefficient (R2) is very similar to 1.

The testing dataset portion was used to assess the model, and then measure the output after the training stage is finished.

Table A2 (Appendix A) shows a comparison between the calculated model using PVGIS and the proposed model. The comparison has been made regarding 40 cities (30 in-sample and ten out-of-sample). As shown in Table A2 (Appendix A), the residual average difference (between the calculated and proposed model) for the tilt angle, azimuth angle, and the three annual irradiations (see Figure 4) is 0.0234, −0.0224, 0.136, 1.41, 0.264, respectively. That comparison demonstrates the effectiveness of the proposed model.

5. Conclusions

The solar energy incident on a PV depends of the tilt angle and orientation. Therefore, they considered a vital factor to obtain maximum solar radiation. It can be concluded that in most cases in the northern hemisphere, solar PV must be directed toward the south, this means that the azimuth angle is equal to zero. Whereas for the southern hemisphere, the solar panels must be directed toward the north, which means that the azimuth angle is equal to 180. So AR1 and AR2 are almost the same for most cities. In general, as the latitude of a specific city increases, it benefits from tilting increases, So the tilt factor increases with increasing latitude.

Neural networks are distinguished by being able to learn and generate an output of their own that is not limited to the feedback they receive. In addition, the network will detect the fault and still generate the output, even though a neuron is not responding, or a piece of information is missing. Therefore, the purpose of this research is to create a simple neural network model that can reliably predict the annual radiation and optimum tilt and azimuth angle in any area of the world and can be easily implemented in a low-cost microcontroller.

It can be concluded that the tilt angle is about or greater than the latitude until the latitude of $30°$, then it becomes less than the latitude until the difference between them reaches more than $20°$. The relation between them is not linear for all the latitudes.

Moreover, this study presents a multi-level world comprehensive neural network model for annual irradiation and PV optimum azimuth and tilt angles. Several simulations were carried out with different evaluation criteria to select the best network topology.

The proposed network topology is composed of two stages. The first stage is to predict the PV optimum tilt and azimuth angle, and the second stage is to predict the AR1, AR2, and AR3. The simulation result shows that the proposed module exhibits excellent performance with an average training MSE of 0.01635. This proposed model can be used in an embedded system or an online system for further PV system analysis and optimization.

Author Contributions: Conceptualization, R.A. A.J. E.N., and S.S.; methodology, R.A., A.J., E.N., and S.S.; software, R.A. and E.N.; validation, A.J., R.A., E.N., and S.S.; formal analysis, E.N. and A.J.; investigation, R.A., A.J., and F.M.-A; writing—original draft preparation, R.A., A.J., E.N., and S.S.; writing—review and editing, F.M.-A., A.J., and S.S. All authors have read and agreed to the published version of the manuscript.

Conflicts of Interest: The authors declare no conflict of interest.

Abbreviations

AR1	Annual Irradiation (kWh/m^2) at optimum tilt angle and orientation
AR2	Annual Irradiation (kWh/m^2) at optimum tilt angle (azimuth angle = 0° for Northern hemisphere and 180° for Southern)
AR3	Annual Irradiation (kWh/m^2) at horizontal surface
CMSAF	Climate Monitoring Satellite Application Facility
DR1	Daily Average Irradiation (kWh/m^2/day) at optimum tilt angle and orientation
DR2	Daily Average Irradiation (kWh/m^2/day) at optimum tilt angle (azimuth angle = 0° for Northern hemisphere and 180° for Southern)
DR3	Daily Average Irradiation (kWh/m^2/day) at horizontal surface
ECMWF	European Centre for Medium-Range Weather Forecasts
F	The tilt factor
MSE	Mean Square Error
NREL	National Solar Irradiation Database
PSO	Particle Swarm Optimization
PV	Photovoltaic

PVGIS	Photovoltaic Geographical Information System
SDGs	Sustainable Development Goals
β	Tilt angle (Degrees)
FFNN	Feed-Forward Neural Networks
LM	Levenberg-Marquardt
AR1	Annual Irradiation (kWh/m^2) at optimum tilt angle and orientation
AR2	Annual Irradiation (kWh/m^2) at optimum tilt angle (azimuth angle = 0 for Northern hemisphere and 180 for Southern)
AR3	Annual Irradiation (kWh/m^2) at horizontal surface
DR1	Daily Average Irradiation (kWh/m^2/day) at optimum tilt angle and orientation
DR2	Daily Average Irradiation (kWh/m^2/day) at optimum tilt angle (azimuth angle = 0 for Northern hemisphere and 180 for Southern)
DR3	Daily Average Irradiation (kWh/m^2/day) at horizontal surface.

Appendix A

Table A1. Optimum tilt and azimuth angles for PV panels, AR1, AR2, AR3, DR1, DR2, and DR3 for all countries of the world.

Country	City	Latitude (deg.)	Longitude (deg.)	Optimum Tilt Angle (deg.)	Azimuth Angle (deg.)	AR1 (kWh/m²)	DR1 (kWh/m²)	AR2 (kWh/m²)	DR2 (kWh/m²)	AR3 (kWh/m²)	DR3 (kWh/m²)	F (Tilt Factor)
Iceland	Reykjavík	64.15	−21.94	49	0	1093.00	2.99	1093.00	2.99	839.15	2.30	1.30
Afghanistan	Kandahar	31.63	65.74	30	−2	2418.44	6.63	2418.29	6.63	2166.78	5.94	1.12
Afghanistan	Kabul	34.56	69.21	31	−8	2228.34	6.11	2226.44	6.10	1981.05	5.43	1.12
Albania	Tirana	41.33	19.82	35	−2	1835.59	5.03	1835.37	5.03	1581.86	4.33	1.16
Albania	Sarande	39.87	20.00	33	2	1939.22	5.31	1939.00	5.31	1694.53	4.64	1.14
Algeria	Algiers	36.75	3.06	31	−4	2014.21	5.52	2013.71	5.52	1788.61	4.90	1.13
Andorra	Andorra La Vella	42.51	1.52	35 (34)	−18	1644.99	4.51	1627.00	4.46	1418.10	3.89	1.15
Angola	Luanda	−8.84	13.29	9	−179	1988.58	5.45	1988.57	5.45	1972.00	5.40	1.01
Antigua and Barbuda	St. Johns	17.12	−61.84	19(18)	−17	2164.31	5.93	2158.43	5.91	2080.39	5.70	1.04
Argentina	Entre Rios	−32.23	−58.69	30	−169	1896.28	5.20	1895.30	5.19	1721.98	4.72	1.10
Argentina	Santa Fe	−29.77	−60.51	28	−169	1917.10	5.25	1915.26	5.25	1760.64	4.82	1.09
Armenia	Yerevan	40.19	44.52	33	−6	1826.76	5.00	1826.36	5.00	1611.18	4.41	1.13
Australia	Perth	−31.95	115.86	29	−176	2165.87	5.93	2165.50	5.93	1965.62	5.39	1.10
Australia	Geraldton	−28.78	114.61	28	−180	2301.10	6.30	2301.10	6.30	2092.13	5.73	1.10
Australia	Karratha	−20.73	116.84	23	−180	2490.05	6.82	2490.05	6.82	2343.49	6.42	1.06
Austria	Vienna	48.21	16.37	38	0	1430.94	3.92	1430.94	3.92	1224.67	3.36	1.17
Austria	Graz	47.07	15.44	39	−2	1503.00	4.12	1502.85	4.12	1270.51	3.48	1.18
Azerbaijan	Baku	40.41	49.87	32	5	1663.83	4.56	1663.05	4.56	1495.81	4.10	1.11
Azerbaijan	Lankaran	38.75	48.85	31	2	1678.76	4.60	1678.55	4.60	1514.72	4.15	1.11
Bahamas	Nassau	25.05	−77.36	25	−5	2104.47	5.77	2104.42	5.77	1958.65	5.37	1.07
Bahrain	Manama	26.22	50.59	26	−1	2404.04	6.59	2404.00	6.59	2230.98	6.11	1.08
Bahrain	Riffa	26.13	50.54	26	−1	2416.54	6.62	2416.48	6.62	2245.62	6.15	1.08
Bangladesh	Dhaka	23.81	90.41	28	4	1916.26	5.25	1915.32	5.25	1759.41	4.82	1.09
Bangladesh	Chittagong	22.36	91.78	27	8	2036.81	5.58	2034.05	5.57	1872.39	5.13	1.09

Table A1. *Cont.*

Barbados	Bridgetown	13.11	−59.61	15	−27	2107.36	5.77	2098.29	5.75	2058.16	5.64	1.02
Belgium	Brussels	50.85	4.35	39	0	1258.11	3.45	1258.11	3.45	1076.91	2.95	1.17
Belgium	Saint Hubert	50.03	5.37	36	0	1198.90	3.28	1198.90	3.28	1049.61	2.88	1.14
Belize	Belmopan	17.25	−88.76	17	7	1907.61	5.23	1906.68	5.22	1850.78	5.07	1.03
Belize	Belize City	17.50	−88.20	18	4	2056.07	5.63	2055.63	5.63	1983.43	5.43	1.04
Benin	Port Novo	6.50	2.63	11	27	1932.30	5.29	1927.88	5.28	1906.39	5.22	1.01
Bhutan	Thimphu	27.47	89.63	31	−15	1913.66	5.24	1902.28	5.21	1704.45	4.67	1.12
Bolivia	Sucre	−19.04	−65.26	23	−180	2433.17	6.67	2433.17	6.67	2280.76	6.25	1.07
Bolivia	La Paz	−16.49	−68.12	21	−180	2285.57	6.26	2285.57	6.26	2165.62	5.93	1.06
Bosnia Herzegovina	Sarajevo	43.86	18.41	34	−5	1431.11	3.92	1430.05	3.92	1258.74	3.45	1.14
Bosnia Herzegovina	Banja Luka	44.77	17.19	35	−4	1458.17	3.99	1457.45	3.99	1274.61	3.49	1.14
Botswana	Gaborone	−24.63	25.92	29	−180	2352.15	6.44	2352.15	6.44	2135.01	5.85	1.10
Brazil	Brasilia	−15.83	−47.92	23	−180	2112.59	5.79	2112.59	5.79	1997.21	5.47	1.06
Brazil	Rio De Janeiro	−22.91	−43.17	24	−180	1872.95	5.13	1872.95	5.13	1755.27	4.81	1.07
Brazil	Manaus	−3.12	−60.02	7	−180	1780.18	4.88	1780.18	4.88	1772.99	4.86	1.00
Brunei Darussalam	Bandar Seri Begawan	4.90	114.94	5	47	1849.17	5.07	1845.30	5.06	1841.85	5.05	1.00
Bulgaria	Sofia	42.70	23.32	35	−4	1605.33	4.40	1605.16	4.40	1404.10	3.85	1.14
Bulgaria	Plovdiv	42.14	24.75	35	0	1701.22	4.66	1701.22	4.66	1479.08	4.05	1.15
Burkina Faso	Ouagadougou	12.37	−1.52	16	0	2356.42	6.46	2356.42	6.46	2282.11	6.25	1.03
Burkina Faso	Banfora	10.64	−4.76	15	1	2274.34	6.23	2274.07	6.23	2214.97	6.07	1.03
Burundi	Gitega	−3.43	29.92	7	−180	1903.71	5.22	1903.71	5.22	1893.34	5.19	1.01
Burundi	Bujumbura	−3.36	29.36	8	−180	1982.06	5.43	1982.06	5.43	1970.43	5.40	1.01
Cabo Verde	Praia	15.00	−23.51	15	3	2263.18	6.20	2262.90	6.20	2205.96	6.04	1.03
Cambodia	Phnom Penh	11.56	104.93	14	0	1932.87	5.30	1932.87	5.30	1893.75	5.19	1.02
Cameroon	Yaounde	3.85	11.50	7	35	1882.09	5.16	1877.84	5.14	1867.71	5.12	1.01
Cameroon	Douala	4.05	9.77	12	43	1784.62	4.89	1772.88	4.86	1762.26	4.83	1.01
Canada	Ottawa	45.42	−75.70	37	0	1563.56	4.28	1563.56	4.28	1325.33	3.63	1.18
Canada	Montreal	45.50	−73.57	37	5	1535.22	4.21	1533.93	4.20	1302.97	3.57	1.18

Table A1. *Cont.*

Canada	Calgary	51.04	−114.07	43	−4	1592.94	4.36	1592.13	4.36	1268.46	3.48	1.26
Canada	Vancouver	49.28	−123.12	38	6	1403.44	3.85	1401.30	3.84	1186.43	3.25	1.18
Central Afr. Republic	Bangui	4.39	18.56	8	21	2037.03	5.58	2034.98	5.58	2021.71	5.54	1.01
Central Afr. Republic	Carnot	4.94	15.88	10	25	2073.25	5.68	2069.33	5.67	2051.33	5.62	1.01
Chad	N'Djamena	12.13	15.06	17	2	2402.55	6.58	2402.16	6.58	2323.50	6.37	1.03
Chile	Arica	−18.48	−70.31	18	−180	2274.32	6.23	2274.32	6.23	2193.16	6.01	1.04
China	Guigang	23.11	109.60	19	17	1400.07	3.84	1396.45	3.83	1354.50	3.71	1.03
China	Kashgar	39.47	75.99	36	2	2009.22	5.50	2008.93	5.50	1720.53	4.71	1.17
China	Lhasa	29.65	91.14	35	−4	2305.73	6.32	2304.28	6.31	1992.22	5.46	1.16
China	Kunming	25.02	102.68	28	4	1745.82	4.78	1745.04	4.78	1605.72	4.40	1.09
Colombia	Bogota	4.71	−74.07	6	0	1684.99	4.62	1684.99	4.62	1678.45	4.60	1.00
Colombia	Medellin	6.254	−75.576	5	−8	1896.07	5.19	1895.95	5.19	1890.18	5.18	1.00
Comoros	Moroni	−11.72	43.25	13	−140	1892.52	5.18	1877.10	5.14	1846.07	5.06	1.02
Republic of the Congo	Brazzaville	−4.27	15.28	4	−180	1877.58	5.14	1877.58	5.14	1874.81	5.14	1.00
Republic of the Congo	Owando	−0.48	15.89	0	−180	1924.80	5.27	1924.80	5.27	1924.80	5.27	1.00
Democratic Republic of the Congo	Kinshasa	−4.44	15.27	5	−180	1841.02	5.04	1841.02	5.04	1837.45	5.03	1.00
Democratic Republic of the Congo	Lubumbashi	−11.69	27.50	19	−180	2286.65	6.26	2286.65	6.26	2195.55	6.02	1.04
Costa-Rica	San José	9.93	−84.09	14	−45	1933.00	5.30	1908.08	5.23	1875.87	5.14	1.02
Croatia	Zagreb	45.82	15.98	35	2	1511.78	4.14	1511.63	4.14	1311.44	3.59	1.15
Croatia	Zadar	44.12	15.23	37	2	1801.18	4.93	1801.08	4.93	1530.99	4.19	1.18
Cuba	Havana	23.11	−82.37	23	−11	2094.01	5.74	2089.25	5.72	1965.96	5.39	1.06
Cuba	Sancti Spiritus	21.93	−79.44	23	−19	2113.43	5.79	2102.92	5.76	1982.22	5.43	1.06
Cyprus	Nicosia	35.19	33.38	31	−2	2167.72	5.94	2167.36	5.94	1928.19	5.28	1.12
Cyprus	Larnaca	34.90	33.62	31	1	2164.18	5.93	2164.12	5.93	1929.96	5.29	1.12
Czech Republic	Prague	50.08	14.44	37	−1	1317.92	3.61	1317.88	3.61	1132.38	3.10	1.16
Czech Republic	Ostrava	49.82	18.26	38	−1	1292.84	3.54	1292.75	3.54	1105.96	3.03	1.17
Denmark	Copenhagen	55.69	12.59	40	2	1261.85	3.46	1261.65	3.46	1050.72	2.88	1.20

Table A1. *Cont.*

Djibouti	Djibouti City	11.57	43.15	14	11	2383.11	6.53	2381.31	6.52	2333.55	6.39	1.02
Dominica	Roseau	15.31	−61.38	15	2	1915.78	5.25	1915.71	5.25	1875.46	5.14	1.02
Dominican Republic	Santo Domingo	18.49	−69.93	20	−13	2084.80	5.71	2080.37	5.70	1989.93	5.45	1.05
Dutch-Antilles	Willemstad	12.11	−68.93	12	7	2208.67	6.05	2208.21	6.05	2171.92	5.95	1.02
Ecuador	Quito	−0.18	−78.47	3	−108	1959.69	5.37	1952.43	5.35	1950.98	5.35	1.00
Egypt	Cairo	30.04	31.24	28	7	2417.65	6.62	2416.13	6.62	2197.43	6.02	1.10
Egypt	Port Said	31.26	32.31	29	3	2316.73	6.35	2314.47	6.34	2093.57	5.74	1.11
Egypt	Aswan	24.09	32.90	25	4	2669.99	7.32	2669.07	7.31	2471.27	6.77	1.08
Egypt	Marsa Matruh	31.35	27.24	27	6	2351.08	6.44	2348.95	6.44	2150.14	5.89	1.09
El Salvador	San Salvador	13.69	−89.22	18	−18	2242.27	6.14	2235.02	6.12	2160.75	5.92	1.03
Equatorial Guinea	Malabo	3.76	8.78	8	19	1676.42	4.59	1675.38	4.59	1664.01	4.56	1.01
Eritrea	Asmara	15.33	38.93	20	0	2339.85	6.41	2339.85	6.41	2236.93	6.13	1.05
Estonia	Tallinn	59.44	24.75	41	1	1119.41	3.07	1119.31	3.07	932.40	2.55	1.20
Estonia	Tartu	58.38	26.73	41	0	1124.62	3.08	1124.62	3.08	943.57	2.59	1.19
Ethiopia	Addis Ababa	8.97	38.73	15	−2	2173.71	5.96	2173.62	5.96	2118.91	5.81	1.03
Ethiopia	Gondar	12.60	37.45	19	−26	2145.84	5.88	2130.39	5.84	2054.75	5.63	1.04
Finland	Helsinki	60.17	24.94	42	3	1125.27	3.08	1124.86	3.08	925.59	2.54	1.22
France	Paris	48.85	2.35	38	−3	1381.32	3.78	1380.65	3.78	1181.09	3.24	1.17
France	Lyon	45.76	4.84	37	1	1578.76	4.33	1578.74	4.33	1348.05	3.69	1.17
France	Rennes	48.114	−1.669	38	0	1413.59	3.87	1413.59	3.87	1210.02	3.32	1.17
France	Bordeaux	44.84	−0.58	37	3	1608.95	4.41	1608.44	4.41	1374.99	3.77	1.17
Gabon	Libreville	0.41	9.47	3	48	1804.25	4.94	1802.80	4.94	1801.52	4.94	1.00
Gabon	Franceville	−1.62	13.60	0	−180	1790.85	4.91	1790.85	4.91	1790.85	4.91	1.00
Gambia	Banjul	13.45	−16.59	16	4	2288.49	6.27	2288.15	6.27	2226.59	6.10	1.03
Georgia	Tbilisi	41.70	44.82	35	4	1737.14	4.76	1736.14	4.76	1509.04	4.13	1.15
Germany	Berlin	52.52	13.38	38	−4	1261.69	3.46	1261.22	3.46	1077.30	2.95	1.17
Germany	Cologne	50.94	6.96	38	−2	1257.92	3.45	1257.79	3.45	1072.06	2.94	1.17
Germany	Munich	48.14	11.58	38	1	1372.50	3.76	1372.46	3.76	1169.59	3.20	1.17
Germany	Hamburg	53.55	9.99	38	−1	1185.43	3.25	1185.34	3.25	1011.99	2.77	1.17

Table A1. *Cont.*

Ghana	Accra	5.60	−0.19	9	28	2131.69	5.84	2126.79	5.83	2109.18	5.78	1.01
Gibraltar	Catalan Bay	36.14	−5.34	31	−27	1884.42	5.16	1845.21	5.06	1654.38	4.53	1.12
Greece	Athens	37.98	23.73	32	2	2055.37	5.63	2055.21	5.63	1818.83	4.98	1.13
Guatemala	Guatemala City	14.63	−90.51	18	−2	2007.60	5.50	2007.56	5.50	1939.68	5.31	1.03
Guinea	Kindia	10.04	−12.86	15	9	2135.68	5.85	2134.46	5.85	2085.93	5.71	1.02
Guinea	Kankan	10.38	−9.31	15	9	2256.01	6.18	2254.54	6.18	2202.55	6.03	1.02
Guinea-Bissau	Bissau	11.86	−15.58	14	5	2223.35	6.09	2222.89	6.09	2169.36	5.94	1.02
Guyana	Georgetown	6.80	−58.16	7	−14	2004.88	5.49	2004.09	5.49	1993.37	5.46	1.01
Haiti	Port-Au-Prince	18.55	−72.34	21	−16	2244.58	6.15	2235.80	6.13	2124.32	5.82	1.05
Honduras	Tegucigalpa	14.07	−87.17	16	1	1956.36	5.36	1956.34	5.36	1905.88	5.22	1.03
Honduras	Catacamas	14.84	−85.88	14	−7	1886.46	5.17	1885.78	5.17	1845.84	5.06	1.02
Hong Kong	Hong Kong	22.42	114.16	20	13	1523.23	4.17	1520.24	4.17	1463.19	4.01	1.04
Hungary	Budapest	47.50	19.04	37	−5	1512.04	4.14	1510.81	4.14	1298.57	3.56	1.16
Hungary	Debrecen	47.53	21.63	37	0	1502.57	4.12	1502.57	4.12	1288.64	3.53	1.17
India	New Delhi	28.61	77.21	31	3	2138.18	5.86	2137.84	5.86	1921.33	5.26	1.11
India	Rajkot	22.30	70.80	27	−1	2300.66	6.30	2300.64	6.30	2108.29	5.78	1.09
India	Jodhpur	26.293	73.034	30	0	2324.87	6.37	2324.87	6.37	2098.01	5.75	1.11
India	Chennai	13.08	80.27	15	3	2137.98	5.86	2137.87	5.86	2088.66	5.72	1.02
India	Nagercoil	8.18	77.41	9	1	2166.94	5.94	2166.92	5.94	2143.62	5.87	1.01
Indonesia	Jakarta	−6.17	106.83	10	−180	1852.98	5.08	1852.98	5.08	1835.41	5.03	1.01
Indonesia	Balikpapan	−1.24	116.85	4	114	1685.95	4.62	1678.05	4.60	1675.83	4.59	1.00
Iran	Tehran	35.69	51.42	32	−2	2083.70	5.71	2083.35	5.71	1850.42	5.07	1.13
Iran	Tabriz	38.09	46.27	32	−10	2025.04	5.55	2023.06	5.54	1795.77	4.92	1.13
Iran	Yazd	31.90	54.36	31	−3	2453.82	6.72	2453.18	6.72	2183.47	5.98	1.12
Iraq	Baghdad	33.32	44.37	31	1	2280.20	6.25	2280.20	6.25	2038.03	5.58	1.12
Iraq	Mosul	36.35	43.15	32	0	2178.96	5.97	2178.96	5.97	1928.69	5.28	1.13
Iraq	Basrah	30.52	47.80	29	0	2324.75	6.37	2324.75	6.37	2117.19	5.80	1.10
Ireland	Dublin	53.35	−6.27	40	−3	1144.43	3.14	1144.21	3.13	968.59	2.65	1.18
Ireland	Kilkenny	52.65	−7.25	38	−1	1129.48	3.09	1129.44	3.09	973.43	2.67	1.16

Table A1. *Cont.*

Israel	Haifa	32.79	34.99	29	6	2167.67	5.94	2165.42	5.93	1958.53	5.37	1.11
Israel	Eilat	29.56	34.95	29	3	2526.58	6.92	2525.82	6.92	2280.23	6.25	1.11
Italy	Rome	41.90	12.50	36	2	1935.18	5.30	1935.05	5.30	1653.95	4.53	1.17
Italy	Catania	37.51	15.08	33	−4	2049.02	5.61	2047.78	5.61	1804.48	4.94	1.13
Ivory Coast	Yamoussoukro	6.83	−5.29	10	36	2001.01	5.48	1991.39	5.46	1970.58	5.40	1.01
Jamaica	Kingston	18.02	−76.80	19	−24	2020.66	5.54	2007.25	5.50	1933.03	5.30	1.04
Jordan	Amman	31.95	35.91	28	4	2313.66	6.34	2312.82	6.34	2102.64	5.76	1.10
Jordan	Zarqa	32.063	36.09	28	2	2315.94	6.35	2315.57	6.34	2101.66	5.76	1.10
Jordan	Irbid	32.56	35.85	9	7	2268.95	6.22	2266.16	6.21	2049.04	5.61	1.11
Kazakhstan	Nur-Sultan	51.16	71.47	38	−5	1442.67	3.95	1442.49	3.95	1231.44	3.37	1.17
Kazakhstan	Zhezqazghan	47.80	67.70	36	−3	1646.43	4.51	1645.54	4.51	1416.89	3.88	1.16
Kenya	Nairobi	−1.29	36.82	0	0	1998.16	5.47	1998.16	5.47	1998.16	5.47	1.00
Kosovo	Prishtina	42.66	21.17	30	0	1613.38	4.42	1613.38	4.42	1419.47	3.89	1.14
Kuwait	Kuwait City	29.38	47.98	28	−1	2380.38	6.52	2380.37	6.52	2173.16	5.95	1.10
Kyrgyz Republic	Bishkek	42.87	74.57	35	−1	1782.39	4.88	1782.30	4.88	1550.76	4.25	1.15
Kyrgyz Republic	Jalal-Abad	40.93	72.98	33.00	2	1882.07	5.16	1881.77	5.16	1656.30	4.54	1.14
Laos	Vientiane	17.98	102.63	23.00	11	1961.04	5.37	1956.94	5.36	1852.99	5.08	1.06
Latvia	Riga	56.95	24.11	40	−1	1170.30	3.21	1170.29	3.21	982.95	2.69	1.19
Latvia	Daugavpils	55.87	26.54	38	0	1154.60	3.16	1154.60	3.16	982.60	2.69	1.18
Lebanon	Beirut	33.89	35.50	29	−1	2113.95	5.79	2113.94	5.79	1909.46	5.23	1.11
Lesotho	Maseru	−29.32	27.49	32	−178	2289.04	6.27	2288.99	6.27	2026.68	5.55	1.13
Liberia	Monrovia	6.32	10.81	11	25	1907.17	5.23	1903.23	5.21	1881.63	5.16	1.01
Libyan Arab Jamahiriya	Tripoli	32.89	13.18	30	6	2267.00	6.21	2264.80	6.20	2036.14	5.58	1.11
Liechtenstein	Vaduz	47.14	9.52	37	5	1326.21	3.63	1324.96	3.63	1138.42	3.12	1.16
Lithuania	Vilnius	54.69	25.28	38	−1	1150.50	3.15	1150.41	3.15	985.76	2.70	1.17
Lithuania	Kaunas	54.90	23.890	38	0	1180.46	3.23	1180.46	3.23	1007.24	2.76	1.17
Luxembourg	Luxembourg	49.61	6.13	36	0	1282.81	3.51	1282.81	3.51	1120.82	3.07	1.14
Macedonia	Skopje	42.00	21.44	34	−2	1663.28	4.56	1663.14	4.56	1461.89	4.01	1.14
Macedonia	Bitola	41.03	21.33	32	−6	1630.95	4.47	1629.71	4.46	1456.76	3.99	1.12

Table A1. *Cont.*

Malaysia	Kuala Lumpur	3.14	101.69	2	−66	1802.55	4.94	1799.80	4.93	1799.19	4.93	1.00
Malaysia	Kangar	6.44	100.20	7	−31	1945.97	5.33	1942.29	5.32	1932.41	5.29	1.01
Mali	Bamako	12.64	−8.00	17	2	2332.23	6.39	2332.18	6.39	2261.85	6.20	1.03
Malta	Valletta	35.90	14.51	31	8	2098.64	5.75	2097.52	5.75	1875.20	5.14	1.12
Mauritania	Nouakchott	18.07	−15.96	19	6	2456.65	6.73	2456.08	6.73	2360.03	6.47	1.04
Mauritius	Port Louis	−20.16	57.50	20	−165	2079.81	5.70	2076.19	5.69	1987.61	5.45	1.04
Mexico	Mexico City	19.43	−99.13	22	−18	2211.22	6.06	2199.60	6.03	2082.58	5.71	1.06
Mexico	Merida	20.97	−89.59	21	−16	2063.70	5.65	2056.68	5.63	1960.02	5.37	1.05
Mexico	Ciudad Juárez	31.69	−106.42	31	0	2484.94	6.81	2484.94	6.81	2190.48	6.00	1.13
Moldova Republic	Chisinau	47.01	28.863	35	0	1508.85	4.13	1508.85	4.13	1310.20	3.59	1.15
Monaco	Monte Carlo	43.74	7.43	38	−1	1895.71	5.19	1895.64	5.19	1579.61	4.33	1.20
Mongolia	Mandalgovi	45.76	106.27	42	0	1895.97	5.19	1895.97	5.19	1534.75	4.20	1.24
Mongolia	Ulgii	48.97	89.970	42	−6	1751.26	4.80	1749.85	4.79	1412.41	3.87	1.24
Montenegro	Podgorica	42.43	19.26	36	1	1854.69	5.08	1854.66	5.08	1581.32	4.33	1.17
Morocco	Rabat	34.02	−6.84	31	7	2196.62	6.02	2192.83	6.01	1947.56	5.34	1.13
Morocco	Casablanca	33.57	−7.59	32	6	2216.54	6.07	2213.90	6.07	1963.28	5.38	1.13
Mozambique	Maputo	−25.97	32.57	29	168	2082.81	5.71	2074.42	5.68	1884.70	5.16	1.10
Mozambique	Lichinga	−13.30	35.25	17	−164	1996.18	5.47	1992.87	5.46	1933.83	5.30	1.03
Myanmar	Naypyitaw	19.76	96.14	26	5	2180.17	5.97	2179.51	5.97	2019.55	5.53	1.08
Myanmar	'Yangon	16.80	96.16	24	−2	1975.38	5.41	1975.27	5.41	1852.94	5.08	1.07
Namibia	Windhoek	−22.57	17.08	27	−173	2473.43	6.78	2471.35	6.77	2266.39	6.21	1.09
Nepal	Kathmandu	27.72	85.32	32	−2	2083.44	5.71	2083.18	5.71	1855.30	5.08	1.12
Netherlands	Amsterdam	52.37	4.89	38	4	1245.27	3.41	1244.87	3.41	1064.77	2.92	1.17
Netherlands	Maastricht	50.85	5.69	38	0	1265.56	3.47	1265.56	3.47	1079.98	2.96	1.17
Nicaragua	Managua	12.15	−86.28	16	−12	2202.59	6.03	2199.97	6.03	2139.88	5.86	1.03
Nicaragua	Rivas	11.44	−85.83	14	1	2113.39	5.79	2113.38	5.79	2066.00	5.66	1.02
Niger	Niamey	13.52	2.13	18	6	2414.85	6.62	2413.94	6.61	2331.02	6.39	1.04
Nigeria	Abuja	9.06	7.49	15	12	2110.16	5.78	2107.84	5.77	2053.46	5.63	1.03
Nigeria	Lagos	6.45	3.40	11	30	1943.48	5.32	1937.03	5.31	1915.62	5.25	1.01

Table A1. *Cont.*

Norway	Oslo	59.91	10.75	43	1	1130.68	3.10	1130.57	3.10	910.76	2.50	1.24
Norway	Tromsø	69.65	18.96	49	9	906.42	2.48	905.73	2.48	713.85	1.96	1.27
Oman	Muscat	23.60	58.54	25	−1	2495.07	6.84	2494.98	6.84	2321.49	6.36	1.07
Oman	Salalah	17.02	54.10	21	4	2383.35	6.53	2382.76	6.53	2258.85	6.19	1.05
Pakistan	Islamabad	33.69	73.06	33	2	2099.78	5.75	2099.36	5.75	1847.45	5.06	1.14
Pakistan	Karachi	24.86	67.01	28	4	2377.52	6.51	2376.65	6.51	2168.84	5.94	1.10
Palestine	Jerusalem	31.78	35.31	28	2	2275.05	6.23	2274.88	6.23	2076.64	5.69	1.10
Palestine	Gaza	31.53	34.46	28	10	2299.91	6.30	2294.36	6.29	2079.07	5.70	1.10
Panama	Panama City	8.98	−79.52	11	−35	1747.42	4.79	1739.50	4.77	1718.60	4.71	1.01
Paraguay	Asuncion	−25.29	−57.62	23	−170	1890.38	5.18	1887.57	5.17	1778.81	4.87	1.06
Peru	Lima	−12.05	77.04	10	155	1761.39	4.83	1757.43	4.81	1741.46	4.77	1.01
Poland	Warsaw	52.23	21.01	38	−3	1273.84	3.49	1273.69	3.49	1086.43	2.98	1.17
Poland	Bielsko-Biala	49.82	19.06	38	−2	1255.06	3.44	1254.91	3.44	1073.01	2.94	1.17
Poland	Gdynia	54.52	18.55	40	0	1249.85	3.42	1249.85	3.42	1051.69	2.88	1.19
Portugal	Lisbon	38.72	−9.14	33	5	1994.31	5.46	1992.69	5.46	1751.20	4.80	1.14
Qatar	Doha	25.29	51.53	25	0	2431.34	6.66	2431.34	6.66	2266.09	6.21	1.07
Romania	Bucharest	44.43	26.10	34	5	1610.98	4.41	1610.02	4.41	1406.15	3.85	1.14
Romania	Craiova	44.315	23.828	35	4	1642.53	4.50	1641.27	4.50	1431.19	3.92	1.15
Romania	Botoșani	47.74	26.67	32	2	1451.10	3.98	1450.93	3.98	1252.32	3.43	1.16
Russia	Saint Petersburg	59.94	30.32	41	3	1076.88	2.95	1076.41	2.95	897.41	2.46	1.20
Russia	Omsk	54.99	73.36	40	−3	1326.81	3.64	1326.34	3.63	1105.67	3.03	1.20
Russia	Barnaul	53.35	83.78	40	−1	1355.12	3.71	1355.10	3.71	1136.97	3.11	1.19
Russia	Murmansk	68.97	33.09	47	−5	866.53	2.37	865.44	2.37	684.00	1.87	1.27
Rwanda	Kigali	−1.94	30.06	4	−167	1930.06	5.29	1929.85	5.29	1926.68	5.28	1.00
Saint Kitts And Nevis	Basseterre	17.30	−62.72	19	−16	2136.25	5.85	2130.80	5.84	2051.04	5.62	1.04
Saint Lucia	Castries	14.01	−60.99	15	−19	2104.18	5.76	2098.57	5.75	2046.02	5.61	1.03
San Marino	San Marino	43.94	12.45	34	9	1592.04	4.36	1587.17	4.35	1394.67	3.82	1.14
Sao Tome & Principe	Sao Tome	0.34	6.73	1	0	1908.00	5.23	1908.00	5.23	1907.91	5.23	1.00
Saudi Arabia	Riyadh	24.63	46.72	25	1	2493.58	6.83	2493.48	6.83	2318.87	6.35	1.08

Table A1. *Cont.*

Saudi Arabia	Jeddah	21.58	39.17	22	15	2488.38	6.82	2479.29	6.79	2344.20	6.42	1.06
Saudi Arabia	Jazan	16.89	42.57	19	0	2394.38	6.56	2394.38	6.56	2300.99	6.30	1.04
Saudi Arabia	Arar	30.98	41.02	29	0	2456.95	6.73	2456.95	6.73	2212.61	6.06	1.11
Senegal	Dakar	14.72	−17.47	17	2	2322.37	6.36	2322.26	6.36	2252.59	6.17	1.03
Serbia	Belgrade	44.82	20.47	36	0	1579.56	4.33	1579.56	4.33	1366.20	3.74	1.16
Seychelles	Victoria	48.43	−123.37	37	5	1547.90	4.24	1546.05	4.24	1317.54	3.61	1.17
Sierra Leone	Koidu	8.62	−10.96	13	26	2068.93	5.67	2063.04	5.65	2027.23	5.55	1.02
Singapore	Singapore	1.29	103.84	0	0	1733.09	4.75	1733.09	4.75	1733.09	4.75	1.00
Slovakia	Bratislava	48.15	17.11	37	0	1466.30	4.02	1466.30	4.02	1256.99	3.44	1.17
Slovakia	Žilina	49.22	18.74	37	−2	1286.53	3.52	1286.41	3.52	1108.48	3.04	1.16
Slovenia	Ljubljana	46.05	14.51	34	12	1428.33	3.91	1420.87	3.89	1247.25	3.42	1.14
Somalia	Mogadishu	2.05	45.32	3	14	2427.88	6.65	2427.64	6.65	2423.50	6.64	1.00
Somalia	Borama	9.94	43.18	14	−24	2459.72	6.74	2450.99	6.72	2397.80	6.57	1.02
South Sudan	Juba	4.85	31.59	8	16	2165.23	5.93	2163.93	5.93	2147.55	5.88	1.01
South Sudan	Renk	11.75	32.811	18	13	2325.21	6.37	2320.93	6.36	2240.34	6.14	1.04
South Africa	Johannesburg	−26.20	28.05	30	180	2256.50	6.18	2256.50	6.18	2020.48	5.54	1.12
South Africa	Durban	−29.855	30.985	33	178	1923.65	5.27	1922.63	5.27	1694.33	4.64	1.13
South Africa	Cape Town	−33.93	18.42	30	173	2160.45	5.92	2157.75	5.91	1944.01	5.33	1.11
Spain	Madrid	40.42	−3.70	36	3	2099.17	5.75	2098.86	5.75	1788.13	4.90	1.17
Spain	Barcelona	41.39	2.17	37	2	1972.30	5.40	1971.63	5.40	1662.81	4.56	1.19
Spain	Málaga	36.72	−4.43	34	5	2142.65	5.87	2141.03	5.87	1869.34	5.12	1.15
Sri-Lanka	Colombo	6.93	79.86	8	−9	2109.74	5.78	2109.31	5.78	2094.87	5.74	1.01
Sri-Lanka	Jaffna	9.66	80.03	8	−8	2153.39	5.90	2153.05	5.90	2138.77	5.86	1.01
St. Vincent/Grenadines	Kingstown	13.16	−61.23	14	−17	2083.32	5.71	2079.13	5.70	2035.39	5.58	1.02
Sudan	Khartoum	15.59	32.54	19	4	2543.61	6.97	2542.19	6.96	2435.33	6.67	1.04
Sudan	El Obeid	13.18	30.22	18	6	2458.61	6.74	2457.59	6.73	2367.66	6.49	1.04
Suriname	Paramaribo	5.85	−55.20	6	−53	1946.84	5.33	1937.57	5.31	1930.37	5.29	1.00
Swaziland	Mbabane	−26.31	31.14	31	177	1928.83	5.28	1927.79	5.28	1724.97	4.73	1.12

Table A1. *Cont.*

Sweden	Stockholm	59.33	18.07	43	1	1172.53	3.21	1172.50	3.21	961.01	2.63	1.22
Sweden	Luleå	65.58	22.16	48	−3	1188.99	3.26	1188.74	3.26	908.70	2.49	1.31
Switzerland	Bern	46.95	7.45	41	2	1592.63	4.36	1592.59	4.36	1291.08	3.54	1.23
Syrian Arab Republic	Damascus	33.51	36.28	31	−8	2335.49	6.40	2334.01	6.39	2073.87	5.68	1.13
Syrian Arab Republic	Homs	34.73	36.716	30	7	2190.91	6.00	2187.95	5.99	1964.10	5.38	1.11
Syrian Arab Republic	Aleppo	36.20	37.13	33	−6	2160.63	5.92	2160.10	5.92	1894.68	5.19	1.14
Tajikistan	Dushanbe	38.56	68.79	31	−4	1867.17	5.12	1866.30	5.11	1665.90	4.56	1.12
Tanzania	Dodoma	−6.16	35.75	8	160	2365.45	6.48	2362.99	6.47	2346.13	6.43	1.01
Tanzania	Songea	−10.65	35.64	12	168	2025.61	5.55	2024.03	5.55	1994.46	5.46	1.01
Thailand	Bangkok	13.76	100.50	17	0	1994.13	5.46	1994.13	5.46	1935.70	5.30	1.03
Thailand	Mueang Chiang Rai	19.91	99.84	25	9	2009.07	5.50	2006.42	5.50	1880.23	5.15	1.07
Togo	Lome	6.13	1.23	9	20	2135.78	5.85	2133.33	5.84	2112.99	5.79	1.01
Togo	Dapaong	10.87	0.20	16	5	2271.33	6.22	2270.77	6.22	2207.94	6.05	1.03
Trinidad and Tobago	Port of Spain	10.66	−61.51	11	−37	1973.87	5.41	1961.97	5.38	1938.35	5.31	1.01
Tunisia	Tunis	36.81	10.18	32	2	2055.49	5.63	2054.98	5.63	1824.57	5.00	1.13
Turkey	Ankara	39.93	32.86	32	−4	1856.34	5.09	1855.51	5.08	1642.72	4.50	1.13
Turkey	İstanbul	41.01	28.97	32	11	1746.38	4.78	1741.66	4.77	1551.90	4.25	1.12
Turkey	Hakkâri	37.58	43.74	29	−5	1896.31	5.20	1895.59	5.19	1722.17	4.72	1.10
Turkmenistan	Ashgabat	37.94	58.39	32	0	1975.89	5.41	1975.89	5.41	1752.51	4.80	1.13
Uganda	Kampala	0.35	32.58	1	74	1955.52	5.36	1953.95	5.35	1953.69	5.35	1.00
Ukraine	Kyiv	50.45	30.52	36	1	1357.97	3.72	1357.93	3.72	1173.62	3.22	1.16
Ukraine	Lviv	49.848	24.033	37	1	1304.11	3.57	1304.03	3.57	1123.40	3.08	1.16
Ukraine	Odessa	46.48	30.72	35	4	1574.72	4.31	1574.14	4.31	1366.41	3.74	1.15
United States	Washington, D.C	38.91	−77.04	35	1	1763.08	4.83	1762.92	4.83	1525.77	4.18	1.16
United States	Minot, ND	48.23	−101.29	42	5	1674.01	4.59	1673.38	4.58	1359.81	3.73	1.23
United States	San Antonio, TX	29.42	−98.49	28	7	2023.09	5.54	2020.54	5.54	1851.56	5.07	1.09
United States	Los Angeles, CA	34.05	−118.24	32	12	2247.35	6.16	2238.74	6.13	1966.44	5.39	1.14
United Arab Emirates	Abu Dhabi	24.43	54.65	25	1	2481.46	6.80	2481.38	6.80	2309.42	6.33	1.07

Table A1. *Cont.*

United Arab Emirates	Dubai	25.27	55.30	25	1	2457.38	6.73	2457.36	6.73	2277.89	6.24	1.08
United Kingdom	London	51.507	−0.128	39	−3	1227.62	3.36	1227.42	3.36	1046.30	2.87	1.17
United Kingdom	York	53.96	−1.087	40	−1	1142.40	3.13	1142.34	3.13	967.71	2.65	1.18
United Kingdom	Truro	50.26	−5.05	37	6	1269.16	3.48	1268.19	3.47	1097.53	3.01	1.16
Uruguay	Montevideo	−34.91	−56.19	30	−177	1802.71	4.94	1801.84	4.94	1622.85	4.45	1.11
Uruguay	Tacuarembo	−31.711	−55.964	29	−176	1814.57	4.97	1814.47	4.97	1664.21	4.56	1.09
Uzbekistan	Tashkent	41.30	69.24	33	0	1924.70	5.27	1924.70	5.27	1692.18	4.64	1.14
Vatican City	Vatican City	41.90	12.45	36	2	1935.25	5.30	1935.14	5.30	1653.96	4.53	1.17
Venezuela	Caracas	10.48	−66.90	11	−17	1952.14	5.35	1949.93	5.34	1927.48	5.28	1.01
Venezuela	Amazonas	2.81	−65.10	4	0	1998.58	5.48	1998.58	5.48	1995.50	5.47	1.00
Vietnam	Hanoi	21.03	105.83	16	28	1483.03	4.06	1475.95	4.04	1446.40	3.96	1.02
Vietnam	Cà Mau	9.18	105.15	11	−25	1849.86	5.07	1845.96	5.06	1826.08	5.00	1.01
Yemen	Sana'A	15.37	44.19	19	−23	2384.73	6.53	2370.25	6.49	2275.92	6.24	1.04
Yemen	Aden	12.79	45.02	15	5	2430.15	6.66	2429.76	6.66	2365.05	6.48	1.03
Zambia	Lusaka	−15.42	28.29	22	−176	2252.38	6.17	2252.05	6.17	2137.47	5.86	1.05
Zimbabwe	Harare	−17.83	31.03	24	−174	2270.50	6.22	2269.35	6.22	2131.28	5.84	1.06

Table A2. In-sample and out-of-sample proposed model performance.

Location Coordinates						Calculated Model Using PVGIS				Proposed Model Using Neural Network				
Country	City	Latitude (deg.)	Longitude (deg.)	Optimum Tilt Angle (deg.)	Azimuth Angle (deg.)	AR1 (kWh/m^2)	AR2 (kWh/m^2)	AR3 (kWh/m^2)	Optimum Tilt Angle (deg.)	Azimuth Angle (deg.)	AR1 (kWh/m^2)	AR2 (kWh/m^2)	AR3 (kWh/m^2)
						In-Sample Testing Set								
Sweden	Luleå	65.58	22.16	48	−3	1188.99	1188.74	908.7	48.03	−3.138	1219	1219	925.5
Australia	Geraldton	−28.78	114.61	28	−180	2301.1	2301.1	2092.13	28	−180	2301	2301	2092
Norway	Tromsø	69.65	18.96	49	9	906.42	905.73	713.85	48.82	10.86	848.8	860.8	703.4
Rwanda	Kigali	−1.94	30.06	4	−167	1930.06	1929.85	1926.68	4.059	−167.3	1940	1933	1916
Brazil	Rio De Janeiro	−22.91	−43.17	24	−180	1872.95	1872.95	1755.27	24	−180	1873	1873	1755
Burundi	Bujumbura	−3.36	29.36	8	−180	1982.06	1982.06	1970.43	7.978	−179.9	1974	1973	1964
Iraq	Mosul	36.35	43.15	32	0	2178.96	2178.96	1928.69	32	−0.1384	2188	2188	1936
Spain	Málaga	36.72	−4.43	34	5	2142.65	2141.03	1869.34	34	4.687	2156	2157	1870
Chile	Arica	−18.48	−70.31	18	−180	2274.32	2274.32	2193.16	18.08	−180	2237	2241	2161
Finland	Helsinki	60.17	24.94	42	3	1125.27	1124.86	925.59	41.92	3.342	1140	1141	927.7
Somalia	Mogadishu	2.05	45.32	3	14	2427.88	2427.64	2423.5	2.827	14.29	2405	2382	2381
Malaysia	Kuala Lumpur	3.14	101.69	2	−66	1802.55	1799.8	1799.19	1.942	−65.99	1783	1785	1773
Suriname	Paramaribo	5.85	−55.20	6	−53	1946.84	1937.57	1930.37	6.055	−53.1	1907	1894	1894
Benin	Port Novo	6.50	2.63	11	27	1932.3	1927.88	1906.39	11.05	27.2	1923	1918	1897
India	Nagercoil	8.18	77.41	9	1	2166.94	2166.92	2143.62	8.986	1.572	2123	2133	2108
Sri-Lanka	Jaffna	9.66	80.03	8	−8	2153.39	2153.05	2138.77	8.038	−8.211	2173	2165	2157
China	Guigang	23.11	109.60	19	17	1400.07	1396.45	1354.5	18.99	17.11	1392	1389	1347
Lebanon	Beirut	33.89	35.50	29	−1	2113.95	2113.94	1909.46	29.07	−1.031	2118	2118	1912
Malta	Valletta	35.90	14.51	31	8	2098.64	2097.52	1875.2	31.03	7.936	2105	2104	1883

Table A2. *Cont.*

United States	Washington, D.C	38.91	−77.04	35	1	1763.08	1762.92	1525.77	34.85	0.6785	1712	1689	1552
Italy	Rome	41.90	12.50	36	2	1935.18	1935.05	1653.95	36.13	2.23	1925	1924	1645
Croatia	Zadar	44.12	15.23	37	2	1801.18	1801.08	1530.99	36.99	2.03	1799	1799	1530
Canada	Ottawa	45.42	−75.70	37	0	1563.56	1563.56	1325.33	36.95	0.0682	1563	1560	1341
Liechtenstein	Vaduz	47.14	9.52	37	5	1326.21	1324.96	1138.42	37	4.99	1326	1325	1139
Germany	Munich	48.14	11.58	38	1	1372.5	1372.46	1169.59	37.99	1.023	1373	1373	1170
Belize	Belmopan	17.25	−88.76	17	7	1907.61	1906.68	1850.78	17	7.008	1907	1906	1850
Bhutan	Thimphu	27.47	89.63	31	−15	1913.66	1902.28	1704.45	31.06	−15.16	1926	1913	1711
Australia	Karratha	−20.73	116.84	23	−180	2490.05	2490.05	2343.49	22.99	−180.9	2520	2494	2339
South Africa	Johannesburg	−26.20	28.05	30	180	2256.5	2256.5	2020.48	29.94	179.8	2262	2265	2026
Namibia	Windhoek	−22.57	17.08	27	−173	2473.43	2471.35	2266.39	26.99	−173.1	2466	2468	2256
Out-of-Sample Testing Set												
Egypt	Port Said	31.263	32.308	29	3	2316.73	2314.47	2093.57	28.98	3	2315	2313	2093
Jordan	Zarqa	32.063	36.09	28	2	2315.94	2315.57	2101.66	27.32	2.042	2474	2477	2226
Syrian Arab Republic	Homs	34.73	36.716	30	7	2190.91	2187.95	1964.1	30	6.999	2191	2188	1964
Romania	Craiova	44.315	23.828	35	4	1642.53	1641.27	1431.19	35	4.001	1643	1641	1431
Ukraine	Lviv	49.848	24.033	37	1	1304.11	1304.03	1123.4	37	1	1304	1304	1123
South Africa	Durban	−29.855	30.985	33	178	1923.65	1922.63	1694.33	33	178	1924	1923	1694
France	Rennes	48.114	−1.669	38	0	1413.59	1413.59	1210.02	38	0.00012	1414	1414	1210
Colombia	Medellin	6.254	−75.576	5	−8	1896.07	1895.95	1890.18	5	−8	1896	1896	1890
India	Jodhpur	26.293	73.034	30	0	2324.87	2324.87	2098.01	30	0.0005	2325	2325	2098
Uruguay	Tacuarembo	−31.711	−55.964	29	−176	1814.57	1814.47	1664.21	29	−176	1815	1814	1664

AR1: annual irradiation (kWh/m^2) at optimum tilt angle and orientation. AR2: annual irradiation (kWh/m^2) at optimum tilt angle (azimuth angle = 0 for Northern Hemisphere and 180 for Southern). AR3: annual irradiation (kWh/m^2) at horizontal surface. DR1: daily average irradiation (kWh/m^2/day) at optimum tilt angle and orientation. DR2: daily average irradiation (kWh/m^2/day) at optimum tilt angle (azimuth angle = 0 for Northern Hemisphere and 180 for Southern). DR3: daily average irradiation (kWh/m^2/day) at horizontal surface.

References

1. Hernandez-Escobedo, Q.; Rodriguez-Garcia, E.; Saldaña-Flores, R.; Fernández-García, A.; Manzano-Agugliaro, F. Solar energy resource assessment in Mexican states along the Gulf of Mexico. *Renew. Sustain. Energy Rev.* **2015**, *43*, 216–238. [CrossRef]

2. Hailu, G.; Fung, A.S. Optimum tilt angle and orientation of photovoltaic thermal system for application in greater Toronto area, Canada. *Sustainability* **2019**, *11*, 6443. [CrossRef]

3. REN21. Renewables 2020 Global Status Report. Paris: REN21 Secretariat. 2020. Available online: https://www.ren21.net/wp-content/uploads/2019/05/gsr_2020_full_report_en.pdf (accessed on 1 December 2020).

4. United Nations General Assembly. *Transforming our World: The 2030 Agenda for Sustainable Development*; Division for Sustainable Development Goals: New York, NY, USA, 2015; pp. 1–35.

5. Dholakia, H.H. Solar powered healthcare in developing countries. *Nat. Energy* **2018**, *3*, 705–707. [CrossRef]

6. Green, M.A.; Dunlop, E.D.; Levi, D.H.; Hohl-Ebinger, J.; Yoshita, M.; Ho-Baillie, A.W. Solar cell efficiency tables (version 56). *Prog. Photovolt. Res. Appl.* **2020**, *28*, 629–638. [CrossRef]

7. Salameh, T.; Tawalbeh, M.; Juaidi, A.; Abdallah, R.; Issa, S.; Alami, A.H. A novel numerical simulation model for the PVT water system in the GCC region. In Proceedings of the 2020 Advances in Science and Engineering Technology International Conferences (ASET), Rome, Italy, 10–11 December 2020; pp. 1–5.

8. Abdallah, R.; Juaidi, A.; Assad, M.; Salameh, T.; Manzano-Agugliaro, F. Energy Recovery from Waste Tires Using Pyrolysis: Palestine as Case of Study. *Energies* **2020**, *13*, 1817. [CrossRef]

9. Salameh, T.; Tawalbeh, M.; Juaidi, A.; Abdallah, R.; Hamid, A.-K. A novel three-dimensional numerical model for PV/T water system in hot climate region. *Renew. Energy* **2020**, *164*, 1320–1333. [CrossRef]

10. Hafez, A.; Soliman, A.; El-Metwally, K.; Ismail, I. Tilt and azimuth angles in solar energy applications—A review. *Renew. Sustain. Energy Rev.* **2017**, *77*, 147–168. [CrossRef]

11. Despotovic, M.; Nedic, V. Comparison of optimum tilt angles of solar collectors determined at yearly, seasonal and monthly levels. *Energy Convers. Manag.* **2015**, *97*, 121–131. [CrossRef]

12. Juaidi, A.; Montoya, F.G.; Ibrik, I.H.; Manzano-Agugliaro, F. An overview of renewable energy potential in Palestine. *Renew. Sustain. Energy Rev.* **2016**, *65*, 943–960. [CrossRef]

13. Juaidi, A.; Montoya, F.G.; Gázquez, J.A.; Manzano-Agugliaro, F. An overview of energy balance compared to sustainable energy in United Arab Emirates. *Renew. Sustain. Energy Rev.* **2016**, *55*, 1195–1209. [CrossRef]

14. Chen, X.M.; Li, Y.; Zhao, B.Y.; Wang, R.Z. Are the optimum angles of photovoltaic systems so important? *Renew. Sustain. Energy Rev.* **2020**, *124*, 109791. [CrossRef]

15. Castellano, N.N.; Parra, J.A.G.; Valls-Guirado, J.; Manzano-Agugliaro, F. Optimal displacement of photovoltaic array's rows using a novel shading model. *Appl. Energy* **2015**, *144*, 1–9. [CrossRef]

16. Takilalte, A.; Harrouni, S.; Yaiche, M.R.; Mora-López, L. New approach to estimate 5-min global solar irradiation data on tilted planes from horizontal measurement. *Renew. Energy* **2020**, *145*, 2477–2488. [CrossRef]

17. Novas, N.; Fernández-García, A.; Manzano-Agugliaro, F. A Simplified Method to Avoid Shadows at Parabolic-Trough Solar Collectors Facilities. *Symmetry* **2020**, *12*, 278. [CrossRef]

18. Racharla, S.; Rajan, K. Solar tracking system—A review. *Int. J. Sustain. Eng.* **2017**, *10*, 72–81.

19. Mousazadeh, H.; Keyhani, A.; Javadi, A.; Mobli, H.; Abrinia, K.; Sharifi, A. A review of principle and sun-tracking methods for maximizing solar systems output. *Renew. Sustain. Energy Rev.* **2009**, *13*, 1800–1818. [CrossRef]

20. Abdallah, R.; Juaidi, A.; Abdel-Fattah, S.; Manzano-Agugliaro, F. Estimating the Optimum Tilt Angles for South-Facing Surfaces in Palestine. *Energies* **2020**, *13*, 623. [CrossRef]

21. Smith, C.J.; Forster, P.M.; Crook, R. An all-sky radiative transfer method to predict optimal tilt and azimuth angle of a solar collector. *Sol. Energy* **2016**, *123*, 88–101. [CrossRef]

22. Le Roux, W.G. Optimum tilt and azimuth angles for fixed solar collectors in South Africa using measured data. *Renew. Energy* **2016**, *96*, 603–612. [CrossRef]

23. Fouad, M.; Shihata, L.A.; Morgan, E.I. An integrated review of factors influencing the performance of photovoltaic panels. *Renew. Sustain. Energy Rev.* **2017**, *80*, 1499–1511. [CrossRef]

24. Photovoltaic Geographical Information System. European Commission. PVGIS (2019). Available online: https://re.jrc.ec.europa.eu/pvg_tools/en/tools.html (accessed on 1 December 2020).

25. Mira, J. Symbols versus connections: 50 years of artificial intelligence. *Neurocomputing* **2008**, *71*, 671–680. [CrossRef]

26. Jyothi, J.; Veena, M.B. An Efficient and Smart Control of Solar Panel Orientation using Machine Learning. In Proceedings of the 2019 Global Conference for Advancement in Technology (GCAT), Bangalore, India, 18–20 October 2019; pp. 1–5.

27. Kim, G.Y.; Han, D.S.; Lee, Z. Solar Panel Tilt Angle Optimization Using Machine Learning Model: A Case Study of Daegu City, South Korea. *Energies* **2020**, *13*, 529. [CrossRef]

28. El-Kassaby, M. Monthly and daily optimum tilt angle for south facing solar collectors; theoretical model, experimental and empirical correlations. *Sol. Wind. Technol.* **1988**, *5*, 589–596. [CrossRef]

29. Morcos, V. Optimum tilt angle and orientation for solar collectors in Assiut, Egypt. *Renew. Energy* **1994**, *4*, 291–298. [CrossRef]

30. Hartley, L.E.; Lozano, J.A.M.; Utrillas, M.; Tena, F.; Pedrós, R. The optimisation of the angle of inclination of a solar collector to maximise the incident solar radiation. *Renew. Energy* **1999**, *17*, 291–309. [CrossRef]

31. Yakup, M.A.B.H.M.; Malik, A. Optimum tilt angle and orientation for solar collector in Brunei Darussalam. *Renew. Energy* **2001**, *24*, 223–234. [CrossRef]

32. Tang, R.; Wu, T. Optimal tilt-angles for solar collectors used in China. *Appl. Energy* **2004**, *79*, 239–248. [CrossRef]

33. Ulgen, K. Optimum tilt angle for solar collectors. *Energy Sources Part A Recovery Util. Environ. Eff.* **2006**, *28*, 1171–1180. [CrossRef]

34. Skeiker, K. Optimum tilt angle and orientation for solar collectors in Syria. *Energy Convers. Manag.* **2009**, *50*, 2439–2448. [CrossRef]

35. Talebizadeh, P.; Mehrabian, M.A.; Abdolzadeh, M. Determination of Optimum Slope Angles of Solar Collectors Based on New Correlations. *Energy Sources Part A Recovery Util. Environ. Eff.* **2011**, *33*, 1567–1580. [CrossRef]

36. Darhmaoui, H.; Lahjouji, D. Latitude Based Model for Tilt Angle Optimization for Solar Collectors in the Mediterranean Region. *Energy Procedia* **2013**, *42*, 426–435. [CrossRef]

37. Khasawneh, Q.A.; Damra, Q.A.; Salman, B.; Husni, O. Determining the Optimum Tilt Angle for Solar Applications in Northern Jordan. *Jordan J. Mech. Ind. Eng.* **2015**, *9*, 187–193.

38. Hartner, M.; Ortner, A.; Hiesl, A.; Haas, R. East to west—The optimal tilt angle and orientation of photovoltaic panels from an electricity system perspective. *Appl. Energy* **2015**, *160*, 94–107. [CrossRef]

39. Safdarian, F.; Nazari, M.E. Optimal tilt angle and orientation for solar collectors in Iran. In Proceedings of the 2015 IEEE 10th International Symposium on Diagnostics for Electrical Machines, Power Electronics and Drives (SDEMPED), Guarda, Portugal, 1–4 September 2015; pp. 494–500.

40. Berisha, X.; Zeqiri, A.; Meha, D. Solar Radiation–The Estimation of the Optimum Tilt Angles for South-Facing Surfaces in Pristina. **2017**. Available online: https://www.google.com.hk/url?sa=t&rct=j&q=&esrc=s&source=web&cd=&ved=2ahUKEwjZoeyVo7PtAhUOA4gKHWNoBC0QFjAEegQIAhAC&url=https%3A%2F%2Fwww.preprints.org%2Fmanuscript%2F201708.0010%2Fv1%2Fdownload&usg=AOvVaw3wBnBGjwMOe3yc41wJimo6 (accessed on 1 December 2020).

41. Guo, M.; Zang, H.; Gao, S.; Chen, T.; Xiao, J.; Cheng, L.; Wei, Z.; Sun, G. Optimal Tilt Angle and Orientation of Photovoltaic Modules Using HS Algorithm in Different Climates of China. *Appl. Sci.* **2017**, *7*, 1028. [CrossRef]

42. Jacobson, M.Z.; Jadhav, V. World estimates of PV optimal tilt angles and ratios of sunlight incident upon tilted and tracked PV panels relative to horizontal panels. *Sol. Energy* **2018**, *169*, 55–66. [CrossRef]

43. Abdulsalam, H.S.; Alibaba, H.Z. Optimum Tilt Angle for Photovoltaic Panels in Famagusta, Cyprus. *IJSSHR* **2019**, *7*, 29–35.

44. Sahu, S.K.; Tripathi, N.; Tripathi, S. A model driven optimization approach to determine tilt angle of solar collector in India. *Int. J. Adv. Res. Eng. Technol.* **2019**, *10*, 2019. [CrossRef]

45. Adu, T.F.; Anto, E.K.; Ramde, E.; Mensah, L.D. Determination of Optimum Tilt Angle for Rooftop Solar Photovoltaic System Installation for KikuKinderhaus in Kumasi. *Int. J. Energy Environ. Sci.* **2020**, *5*, 7. [CrossRef]

46. Kallioğlu, M.A.; Durmuş, A.; Karakaya, H.; Yılmaz, A. Empirical calculation of the optimal tilt angle for solar collectors in northern hemisphere. *Energy Sources Part A Recovery Util. Environ. Eff.* **2020**, *42*, 1335–1358. [CrossRef]

47. Pourfayaz, F.; Shirmohammadi, R.; Maleki, A.; Kasaeian, A. Improvement of solar flat-plate collector performance by optimum tilt angle and minimizing top heat loss coefficient using particle swarm optimization. *Energy Sci. Eng.* **2020**, *8*, 2771–2783. [CrossRef]

48. Sugirianta, I.B.K.; Sunaya, I.; Saputra, I. Optimization of tilt angle on-grid 300Wp PV plant model at Bukit Jimbaran Bali. *J. Phys. Conf. Ser.* **2020**, *1450*, 012135. [CrossRef]

49. Alyami, F.H.; Gomez, P. Semi-Seasonally Optimized Tilt Angles for Design of Utility-Scale Photovoltaic Generation Station. In Proceedings of the 2020 IEEE Texas Power and Energy Conference (TPEC), College Station, TX, USA, 6–7 February 2020; pp. 1–5.

50. Schuster, C.S. The quest for the optimum angular-tilt of terrestrial solar panels or their angle-resolved annual insolation. *Renew. Energy* **2020**, *152*, 1186–1191. [CrossRef]

51. CM SAF: Climate Monitoring Satellite Application Facility. Available online: https://www.cmsaf.eu/EN/Home/home_node.html (accessed on 1 December 2020).

52. NREL: National Solar Radiation Database. Available online: https://nsrdb.nrel.gov/data-sets/archives.html (accessed on 1 December 2020).

53. ECMWF: European Centre for Medium-Range Weather Forecasts. Available online: https://www.ecmwf.int/en/forecasts/documentation-and-support/medium-range-forecasts (accessed on 1 December 2020).

54. Negnevitsky, M. *Artificial Intelligence: A Guide to Intelligent Systems*; Addison-Wesley: Boston, MA, USA, 2004.

55. Yu, H.; Wilamowski, B.M. Levenberg–Marquardt Training. In *The Industrial Electronics Handbook*, 2nd ed.; Intelligent Systems; CRC Press: Boca Raton, FL, USA, 2011; Volume 5, Available online: http://www.eng.auburn.edu/~{}\protect\T1\textbraceleft\protect\T1\textbracerightwilambm/pap/2011/K10149_C012.pdf (accessed on 1 December 2020).

56. Jayalakshmi, T.; Santhakumaran, A. Statistical normalization and back propagation for classification. *Int. J. Comput. Theory Eng.* **2011**, *3*, 1793–8201.

57. Cömert, Z.; Kocamaz, A.F. A Study of Artificial Neural Network Training Algorithms for Classification of Cardiotocography Signals. *Bitlis Eren Univ. J. Sci. Technol.* **2017**, *7*, 93–103. [CrossRef]

58. Samara, S.; Natsheh, E. Intelligent Real-Time Photovoltaic Panel Monitoring System Using Artificial Neural Networks. *IEEE Access* **2019**, *7*, 50287–50299. [CrossRef]

59. Breyer, C.; Schmid, J. Global Distribution of optimal Tilt Angles for fixed tilted PV Systems. In Proceedings of the 25th European Photovoltaic Solar Energy Conference/WCPEC-5, Valencia, Spain, 6–10 September 2010.

60. Zsiborács, H.; Bai, A.; Popp, J.; Gabnai, Z.; Pályi, B.; Farkas, I.; Baranyai, N.H.; Veszelka, M.; Zentkó, L.; Pintér, G. Change of Real and Simulated Energy Production of Certain Photovoltaic Technologies in Relation to Orientation, Tilt Angle and Dual-Axis Sun-Tracking. A Case Study in Hungary. *Sustainability* **2018**, *10*, 1394. [CrossRef]

61. Raskutti, G.; Wainwright, M.J.; Yu, B. Early stopping for non-parametric regression: An optimal data-dependent stopping rule. In Proceedings of the 2011 49th Annual Allerton Conference on Communication, Control, and Computing (Allerton), Monticello, IL, USA, 28–30 September 2011; pp. 1318–1325.